Pola

Tunelowanie

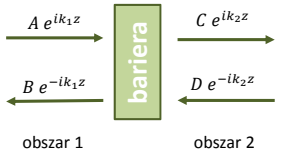

$$\begin{pmatrix} C \\ D \end{pmatrix} = T^{(21)} \begin{pmatrix} A \\ B \end{pmatrix} = \begin{pmatrix} T_{11} & T_{12} \\ T_{12}^* & T_{11}^* \end{pmatrix} \begin{pmatrix} A \\ B \end{pmatrix}$$

$$r = -\frac{T_{12}^*}{T_{11}^*} \qquad t = -\frac{1}{T_{11}^*}$$

$$T^{(21)}(0) = \begin{pmatrix} 1/t^* & -r^*/t^* \\ -r/t & 1/t \end{pmatrix}$$

$$T^{(21)}(d) = \begin{pmatrix} e^{-ik_2 d} & 0 \\ 0 & e^{ik_2 d} \end{pmatrix} T^{(21)}(0) \begin{pmatrix} e^{ik_1 d} & 0 \\ 0 & e^{ik_1 d} \end{pmatrix} = A_2^{-1}(d)\, T(0)\, A_1(d)$$

W drugą stronę: $\begin{pmatrix} B \\ A \end{pmatrix} = T^{(12)} \begin{pmatrix} D \\ C \end{pmatrix}$

$$T^{(12)}(0) = \begin{pmatrix} 1/t^* & r/t \\ r^*/t^* & 1/t \end{pmatrix}$$

Tunelowanie

Przykłady:

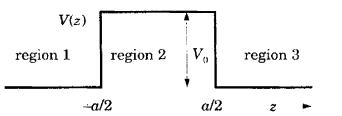

Poziomy nieskończonej anty-studni!

FIGURE 5.5. Potential barrier with $V(z) = V_0$ for $|z| < a/2$ and $V(z) = 0$ elsewhere.

$E > V_0$

$$T = \frac{4k_1^2 k_2^2}{4k_1^2 k_2^2 + (k_1^2 - k_2^2)^2 \sin^2 k_2 a} = \left[1 + \frac{V_0^2}{4E(E - V_0)} \sin^2 k_2 a\right]^{-1}$$

$E < V_0$

$$T = \frac{4k_1^2 \kappa_2^2}{4k_1^2 \kappa_2^2 + (k_1^2 + \kappa_2^2)^2 \sinh^2 k_2 a} = \left[1 + \frac{V_0^2}{4E(V_0 - E)} \sinh^2 \kappa_2 a\right]^{-1}$$

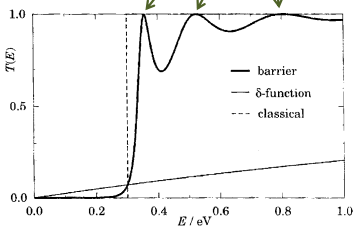

FIGURE 5.6. Transmission coefficient $T(E)$ as a function of energy E for a square potential barrier of height $V_0 = 0.3$ eV and thickness $a = 10$ nm in GaAs. The thin curve is for a δ-function barrier of the same strength $S = V_0 a$, and the broken curve is the classical result for a barrier of the same height.

Tunelowanie

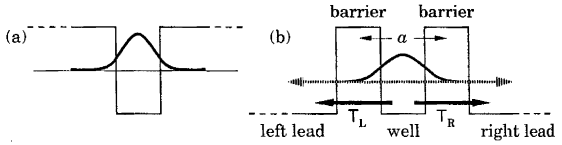

FIGURE 5.10. (a) A finite square potential well with a true bound state. (b) The same well but with barriers of finite thickness, where the bound state becomes resonant or quasi-bound.

$$t = \frac{t_L t_R}{1 - r_L r_R \exp 2ika}$$

$$\phi = 2ka + \rho_L + \rho_R$$

$$T = |t|^2 = \frac{T_L T_R}{\left(1 - \sqrt{R_L R_R}\right)^2 + 4\sqrt{R_L R_R} \sin^2 \frac{1}{2}\phi} \qquad T_{pk} = \frac{T_L T_R}{\left(1 - \sqrt{R_L R_R}\right)^2} \approx \frac{4T_L T_R}{(T_L + T_R)^2}$$

Tunelowanie

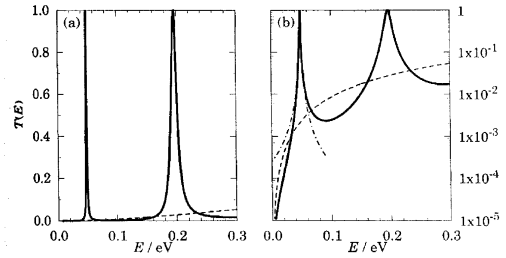

FIGURE 5.11. Transmission coefficient of a resonant-tunnelling structure on (a) linear and (b) logarithmic scales. The barriers are δ-functions of strength 0.3 eV × 5 nm separated by 10 nm. The **solid curve** is $T(E)$ for the whole structure, the dashed curve shows the square of $T(E)$ for a single barrier and would apply to the double-barrier structure if there were no resonance, and the chain **curve** is the Lorentzian approximation to the lowest resonance.

$$T = |t|^2 = \frac{T_L T_R}{\left(1 - \sqrt{R_L R_R}\right)^2 + 4\sqrt{R_L R_R}\sin^2\frac{1}{2}\phi} \qquad T_{pk} = \frac{T_L T_R}{\left(1 - \sqrt{R_L R_R}\right)^2} \approx \frac{4T_L T_R}{(T_L + T_R)^2}$$

Gęstość ładunku i prądu

Gęstość prądu: $J(\vec{r},t) = J(\vec{r}) = \frac{\hbar q}{2\,i\,m}(\Psi^*\nabla\Psi - \Psi\nabla\Psi^*)$

W przypadku fali de Broigla: $\Psi(x,t) = \left[A_+ e^{ikx} + A_- e^{-ikx}\right]e^{-i\omega t}$

$J(\vec{r}) = \frac{\hbar q\,k}{m}(|A_+|^2 - |A_-|^2)$ czyli każda fala niesie z sobą prąd

W przypadku fali zanikającej: $\Psi(x,t) = [B_+ e^{\kappa x} + B_- e^{\kappa x}]e^{-i\omega t}$

$$J(\vec{r}) = \frac{\hbar q\,\kappa}{i\,m}(B_+ B_-^* - B_+^* B_-) = \frac{2\,\hbar q\,\kappa}{m}\mathrm{Im}\,(B_+ B_-^*)$$

Tylko złożenie amplitud + i – daje rzeczywisty prąd!

Fala klasyczna: $\Psi(x,t) = Re\{\left[A_+ e^{ikx} + A_- e^{-ikx}\right]e^{-i\omega t}\}$

Gęstość ładunku i prądu

Gęstość prądu: $J(\vec{r},t) = J(\vec{r}) = \frac{\hbar q}{2\,i\,m}(\Psi^*\nabla\Psi - \Psi\nabla\Psi^*)$

W przypadku fali de Broigla: $\Psi(x,t) = \left[A_+ e^{ikx} + A_- e^{-ikx}\right]e^{-i\omega t}$

$J(\vec{r}) = \frac{\hbar q\,k}{m}(|A_+|^2 - |A_-|^2)$ czyli każda fala niesie z sobą prąd

W przypadku fali zanikającej: $\Psi(x,t) = [B_+ e^{\kappa x} + B_- e^{\kappa x}]e^{-i\omega t}$

$$J(\vec{r}) = \frac{\hbar q\,\kappa}{i\,m}(B_+ B_-^* - B_+^* B_-) = \frac{2\,\hbar q\,\kappa}{m}\mathrm{Im}\,(B_+ B_-^*)$$

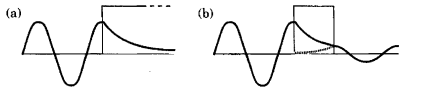

FIGURE 1.5. Current carried by counter-propagating decaying waves. (a) An infinitely thick barrier contains a single decaying exponential that carries no current. (b) A finite barrier contains both growing and decaying exponentials and passes current. (The wave function is complex, so the figure is only a rough guide.)

Tylko złożenie amplitud + i – daje rzeczywisty prąd!

Kwant przewodnictwa

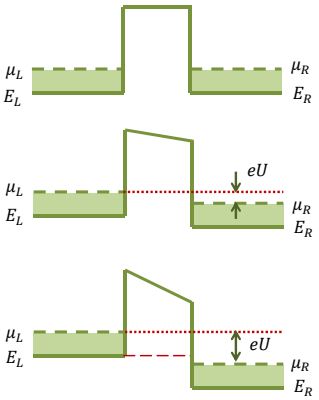

$I = I_L + I_R$

$I_L = \frac{2e}{h}\int_{E_L}^{\infty} f(E,\mu_L)T(E)dE$

$I_R = -\frac{2e}{h}\int_{E_R}^{\infty} f(E,\mu_R)T(E)dE$

$I = \frac{2e}{h}\int_{E_L}^{\infty}[f(E,\mu_L) - f(E,\mu_R)]T(E)dE$

Na ćwiczeniach

$I = \frac{2e}{h}\int_{E_L}^{\infty} f(E,\mu_L)T(E)dE$

Kwant przewodnictwa

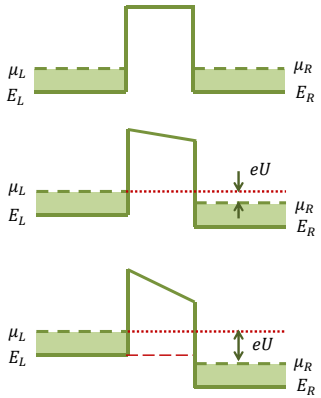

Dla temperatury $T \to 0$:

$$I = \frac{2e}{h}\int_{\mu_R}^{\mu_L}[f(E,\mu_L) - f(E,\mu_R)]T(E)dE$$

$$I = \frac{2e}{h}\int_{E_L}^{\mu_L} f(E,\mu_L)T(E)dE$$

Kwant przewodnictwa

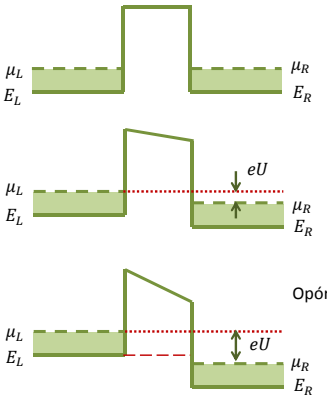

Dla metali $\mu_L = \mu + \frac{1}{2}eU$ i $\mu_R = \mu - \frac{1}{2}eU$:

$$f(E,\mu_L) - f(E,\mu_R) \approx$$
$$\approx eU\frac{\partial f(E,\mu)}{\partial \mu} = -eU\frac{\partial f(E,\mu)}{\partial E}$$

$$I = \frac{2e^2U}{h}\int_{E_L}^{\infty}\frac{\partial f(E,\mu)}{\partial E}T(E)dE$$

$$G = \frac{dI}{dU} = \frac{2e^2}{h}\int_{E_L}^{\infty}\frac{\partial f(E,\mu)}{\partial E}T(E)dE \approx \frac{2e^2}{h}T(\mu)$$

Opór jest skończony nawet dla idealnego przewodnika!

$\frac{e^2}{h} = 38{,}7\ \mu S$ $\qquad$ $\frac{h}{e^2} = 25{,}8\ k\Omega$

Kwant przewodnictwa (w simensach)

Kwant przewodnictwa

$$G = \frac{dI}{dU} = \frac{2e^2}{h}\int_{E_L}^{\infty}\frac{\partial f(E,\mu)}{\partial E}T(E)dE \approx \frac{2e^2}{h}T(\mu) = 2G_0'T(\mu) = G_0T(\mu)$$

$\frac{e^2}{h} = 38{,}7\ \mu S$

To są różne definicje G_0 - częściej jest z 2:
$\frac{2e^2}{h} = 77{,}4\ \mu S$

Wzór Landauera (*Landauer formula*) – gdy mamy do czynienia z wieloma kanałami przewodnictwa

$$G = G_0\sum_n T_n(\mu) \approx NG_0'$$

Trzeba uważać na definicję G_0!

N to suma różnych „pełnych" kanałów przewodnictwa
np. dwa różne spiny dają $N = 2$

Dla $T = const$ dostajemy prawo Ohma.

Studnia trójkątna

Metoda przybliżona WKB (Wentzel – Krammers – Brillouin) – dla potencjału *wolnozmiennego*

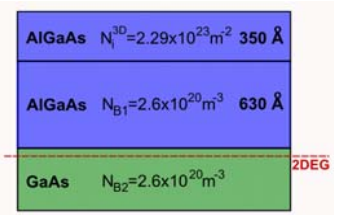

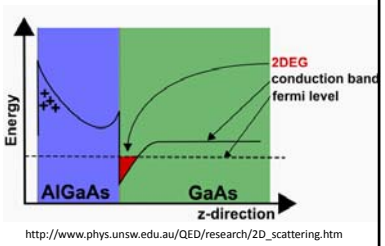

http://www.phys.unsw.edu.au/QED/research/2D_scattering.htm

$$E_n = \left[\frac{3}{2}\pi\left(n - \frac{1}{4}\right)\right]^{2/3}\left[\frac{(eF\hbar)^2}{2m}\right]^{1/3}$$

Studnia trójkątna

Metoda przybliżona WKB (Wentzel – Krammers – Brillouin) – dla potencjału *wolnozmiennego*

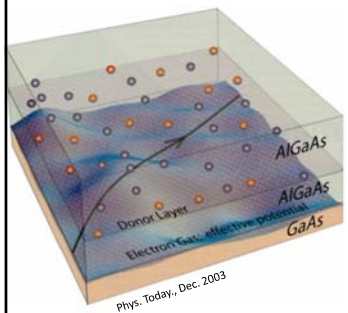

Phys. Today, Dec. 2003

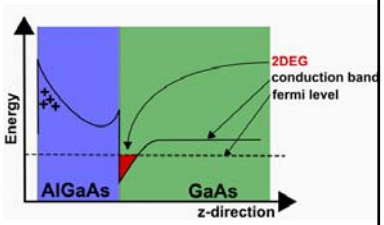

http://www.phys.unsw.edu.au/QED/research/2D_scattering.htm

$$E_n = \left[\frac{3}{2}\pi\left(n-\frac{1}{4}\right)\right]^{2/3}\left[\frac{(eF\hbar)^2}{2m}\right]^{1/3}$$

Kwant przewodnictwa

$$G = \frac{dI}{dU} = \frac{2e^2}{h}\int_{E_L}^{\infty}\frac{\partial f(E,\mu)}{\partial E}T(E)dE \approx \frac{2e^2}{h}T(\mu) = G_0T(\mu)$$

$$\frac{2e^2}{h} = 77{,}5\ \mu S$$

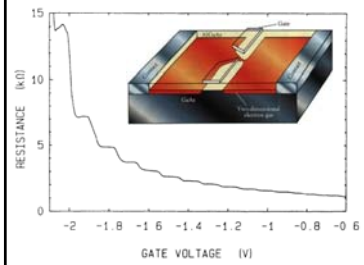

FIG. 1. Point-contact resistance as a function of gate voltage at 0.6 K. Inset: Point-contact layout.

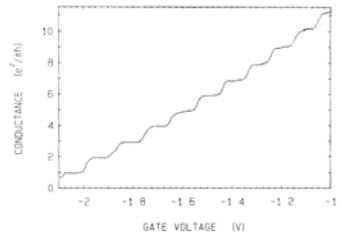

FIG. 2. Point-contact conductance as a function of gate voltage, obtained from the data of Fig. 1 after subtraction of the lead resistance. The conductance shows plateaus at multiples of $e^2/\pi h$.

B. J. van Wees et al. *Quantized conductance of point contacts in a two-dimensional electron gas* Phys. Rev. Lett. **60**, 848–850 (1988)

Kwant przewodnictwa

$$G = \frac{2e^2}{h}T(\mu) = G_0T(\mu)$$

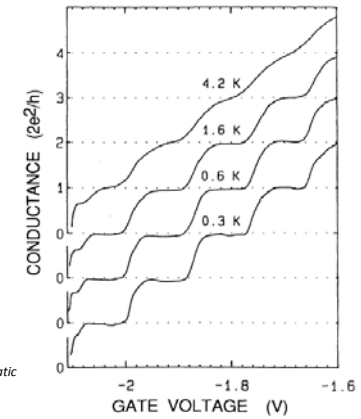

B. J. van Wees et al. *Quantum ballistic and adiabatic electron transport studied with quantum point contacts* Phys. Rev. B 43, 12431–12453 (1991)

FIG. 6. Breakdown of the conductance quantization due to temperature averaging. The curves have been offset for clarity.

Kwant przewodnictwa

$$G = \frac{2e^2}{h}T(\mu) = G_0T(\mu)$$

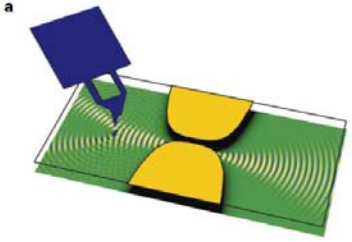

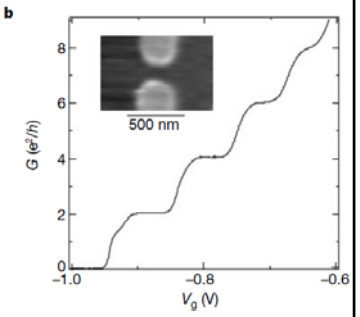

M. A. Topinka et al. *Coherent branched flow in a two-dimensional electron gas* Nature 410, 183 (2001)

Kwant przewodnictwa

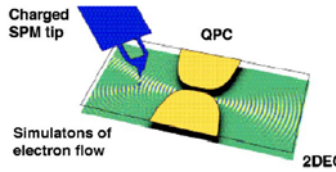

Fig. 1. Schematic diagram showing a negatively charged SPM tip positioned above a quantum point contact (QPC) formed in a two-dimensional electron gas (2DEG) by electrostatic gates. Simulations of electron flow in the diagram show how electron waves are scattered by the depleted disc beneath the tip Topinka et al. [16].

Fig. 2. Experimental images (outside) and theoretical simulations (inside) of the flow of electron waves through a quantum point contact for the first three modes (a)–(c). Fringes spaced by half the Fermi wavelength demonstrate coherence in the flow Topinka et al. [6].

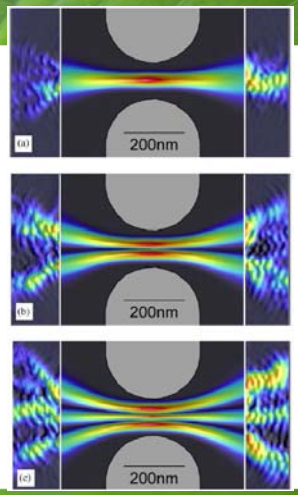

R.M. Westervelt, M. A. Topinka et al.
Physica E 24 (2004) 63–69

Kwant przewodnictwa

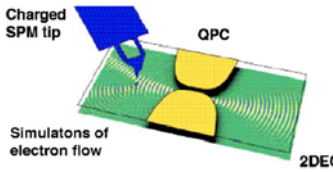

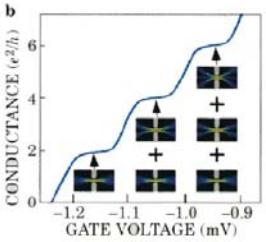

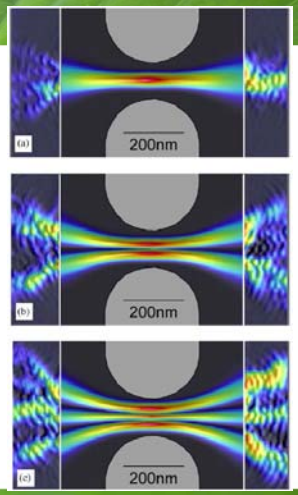

Physica E 24 (2C

Kwant przewodnictwa

$$G = \frac{2e^2}{h} T(\mu) = G_0 T(\mu)$$

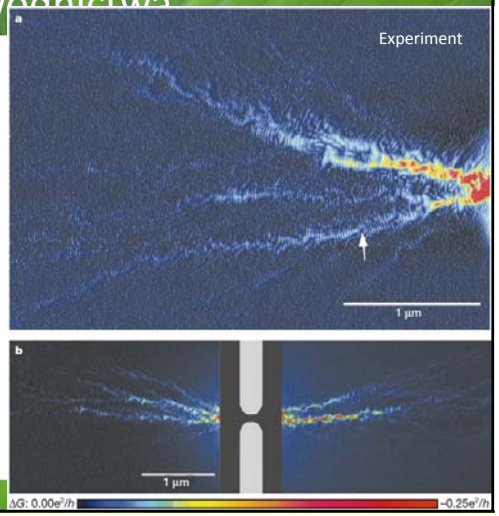

M. A. Topinka et al.
Nature 410, 183 (2001)

Kwant przewodnictwa

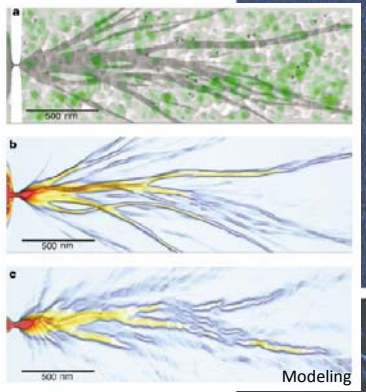

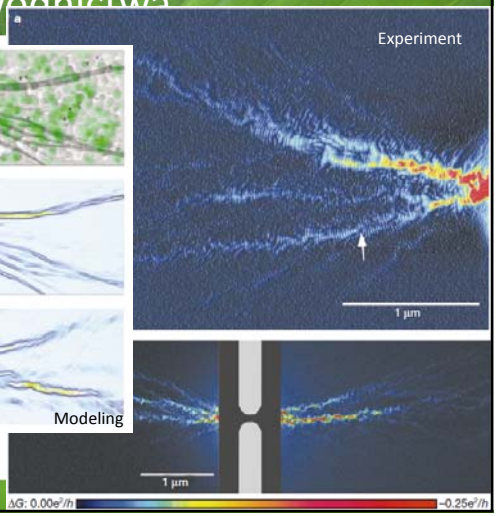

M. A. Topinka et al.
Nature **410**, 183 (2001)

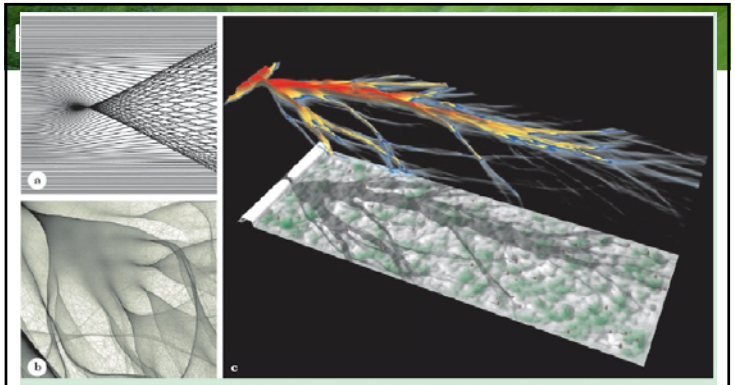

Figure 6. Simulations of electron flow. (a) Parallel electron trajectories, going from left to right, form a V-shaped cusp due to focusing by a potential-energy dip caused by a charged donor atom (not seen) above a two-dimensional electron gas. **(b)** A realistic 2DEG simulation that includes many ionized donors forms several generations of cusps. The electrons travel here from upper left to lower right. **(c)** Ray-tracing simulations of electron flux emerging from a small opening into a region of random potential reflect the features seen in experimental images of 2DEG quantum point contact samples. The potential is shown green in the valleys and white on the peaks. The electron flux is coded by height and color, with blue corresponding to regions of low flux; still lower flux is transparent. The "shadow" of the flux on the potential plot shows where the flux lies relative to the hills and valleys; no guiding valleys are seen. A slight change of the position of the opening changes the location and direction of the branches. (S. E. J. Shaw, PhD thesis, Harvard University, 2002.)

Kwant przewodnictwa

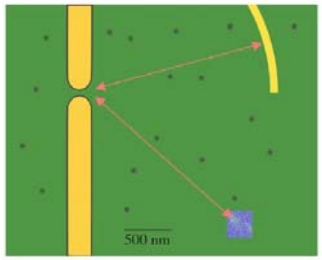

Fig. 3. Schematic diagram showing how a V-shaped electron interferometer was constructed using a QPC and a reflecting gate (gates in gold color). The SPM tip was scanned over the small blue area at approximately the same distance from the QPC as the reflector gate. Electrons passing from the QPC travel along both legs of the interferometer at once (paths shown in red, with arrows), and interfere when they return to their starting point.

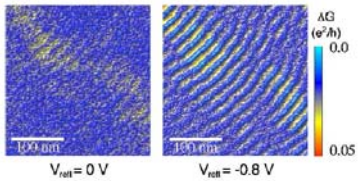

Fig. 4. Experimental images that show that fringes are created in the interferometer of Fig. 3, when the reflector mirror is turned on by depleting the electron gas below. Only weak fringes are observed in the left panel when the reflector mirror is off ($V_{refl} = 0$ V), while strong fringes are observed in the right panel when the reflector mirror is on ($V_{refl} = -0.8$ V).

R.M. Westervelt, M. A. Topinka et al.
Physica E 24 (2004) 63–69

Kwant przewodnictwa

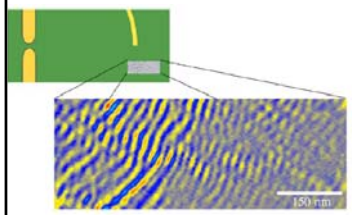

Fig. 6. Image of fringes in an electron interferometer that show how the fringe intensity varies with distance from the QPC—the fringes are strongest at the same distance from the QPC as the reflector mirror. An ensemble average over the thermal distribution of electron energies tends to wash out fringes at other distances.

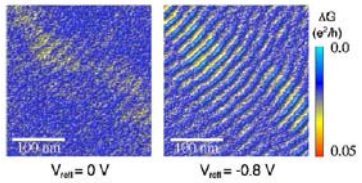

Fig. 4. Experimental images that show that fringes are created in the interferometer of Fig. 3, when the reflector mirror is turned on by depleting the electron gas below. Only weak fringes are observed in the left panel when the reflector mirror is off ($V_{refl} = 0$ V), while strong fringes are observed in the right panel when the reflector mirror is on ($V_{refl} = -0.8$ V).

R.M. Westervelt, M. A. Topinka et al.
Physica E 24 (2004) 63–69

Tunelowanie

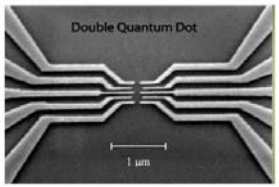

Jeong, Chang, Melloch *Science* **293** 2222 (2001)

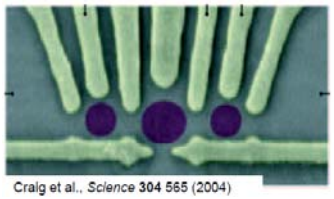

Craig et al., *Science* **304** 565 (2004)

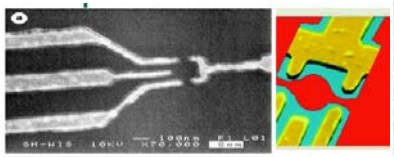

Goldhaber-Gordon *et al. Nature* **391** 156 (1998)

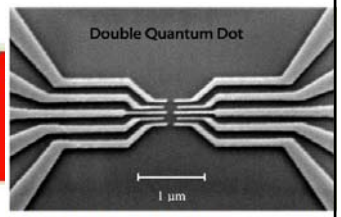

Jeong, Chang, Melloch *Science* **293** 2222 (2001)

Tunelowanie

Kropka zachowuje się jak mały kondensator o energii $E_c \sim \frac{1}{2}\frac{e^2}{C}$

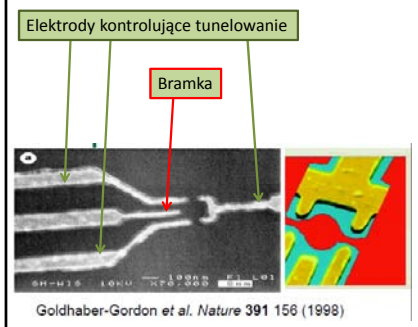

Elektrody kontrolujące tunelowanie

Bramka

Goldhaber-Gordon *et al. Nature* **391** 156 (1998)

$V_G = 0$

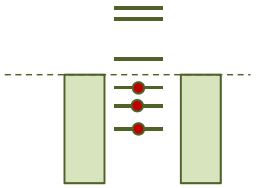

Blokada Kulombowska

Kropka zachowuje się jak mały kondensator o energii $E_c \sim \frac{1}{2}\frac{e^2}{C}$

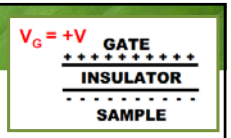

$V_G = 0$ $V_G = +V$ $V_G = -V$

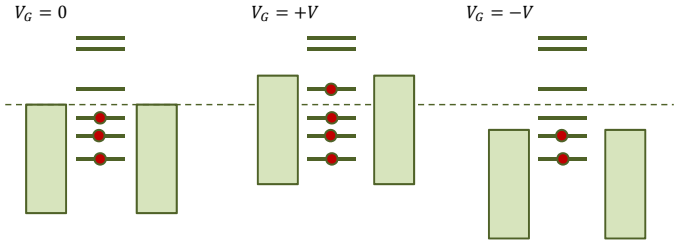

Blokada Kulombowska

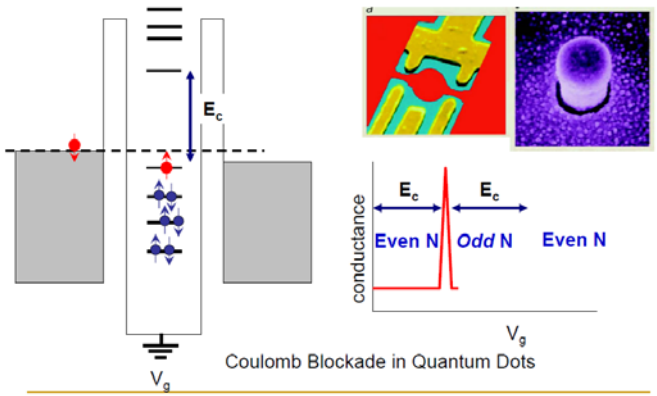

Coulomb Blockade in Quantum Dots

Y. Alhassid *Rev. Mod. Phys.* **72** 895 (2000).

http://sces.phys.utk.edu/~dagotto/condensed/Lectures_2008/UTK_Lecture1_March08.pdf

Luis Dias – UT/ORNL

Blokada Kulombowska

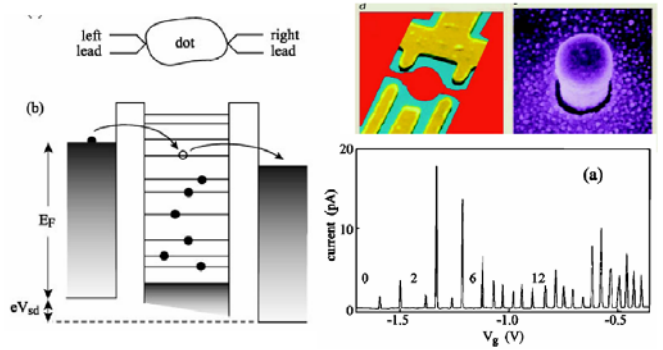

Coulomb Blockade in Quantum Dots: "dot spectroscopy"

http://sces.phys.utk.edu/~dagotto/condensed/Lectures_2008/UTK_Lecture1_March08.pdf

Luis Dias – UT/ORNL

Blokada Kulombowska

Kropka zachowuje się jak mały kondensator o energii $E_c \sim \frac{1}{2}\frac{e^2}{C}$

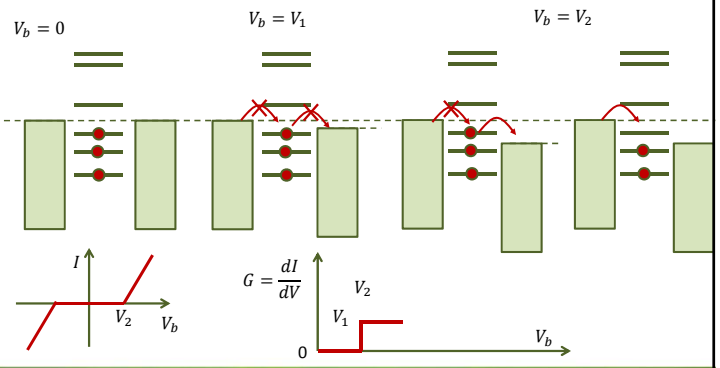

Blokada Kulombowska

Kropka zachowuje się jak mały kondensator o energii $E_c \sim \frac{1}{2}\frac{e^2}{C}$

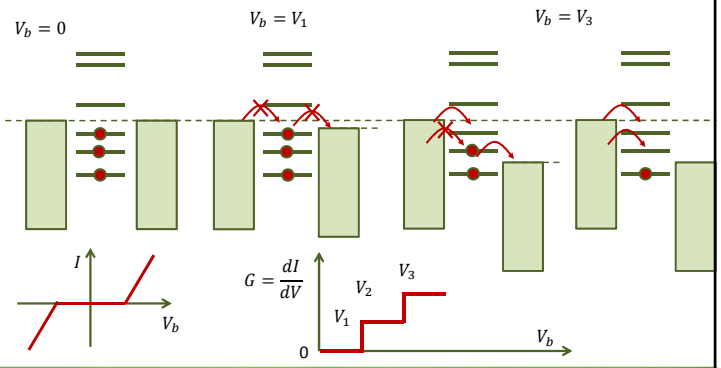

Blokada Kulombowska

Kropka zachowuje się jak mały kondensator o energii $E_c \sim \frac{1}{2}\frac{e^2}{C}$

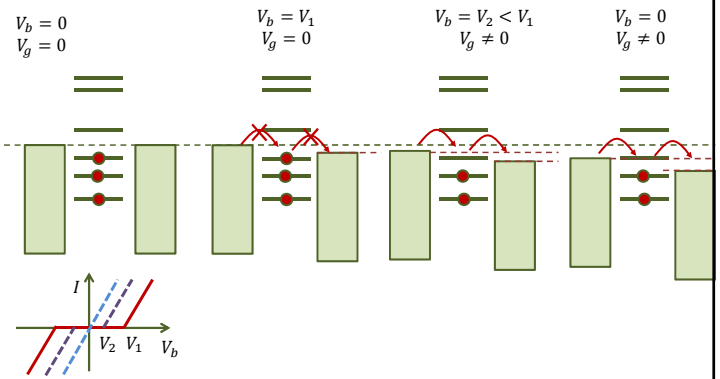

Blokada Kulombowska

Kropka zachowuje się jak mały kondensator o energii $E_c \sim \frac{1}{2}\frac{e^2}{C}$

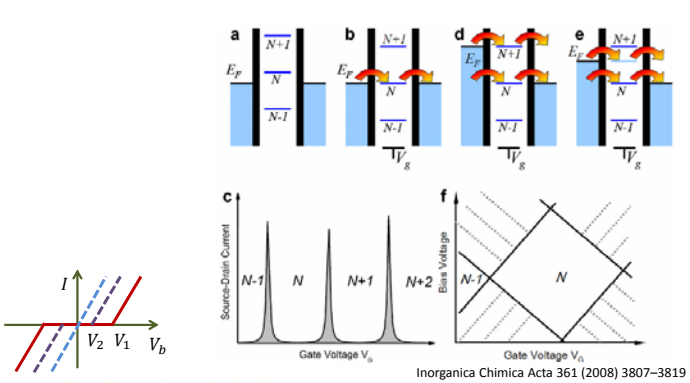

Inorganica Chimica Acta 361 (2008) 3807–3819

Blokada Kulombowska

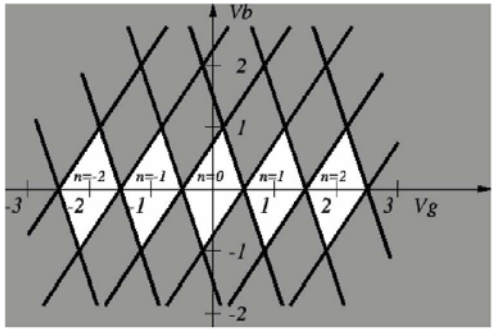

Figure 6: "Coulomb diamonds"

http://www.dstuns.iitm.ac.in/teaching-and-presentations/teaching/undergraduate%20courses/vy305-molecular-architecture-and-evolution-of-functions/presentations/presentations-2007/seminar-2/P2.pdf

Blokada Kulombowska

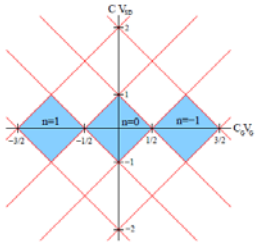

Figure 6.6: A stability diagram for a SET. The blue shaded regions are the Coulomb diamonds, where the number of electrons on the dot is fixed at n and transport through the dot is blocked. Red lines indicate voltages where the number of addition energies within the transport window changes by one. We have set $\epsilon = 1$ here for convenience.

Clive Emary
Theory of Nanostructures nanoskript.pdf

Blokada Kulombowska

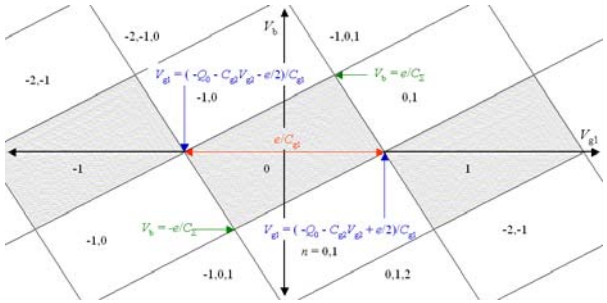

http://lamp.tu-graz.ac.at/~hadley/ss2/set/transistor/coulombblockade.php

Blokada Kulombowska

Excitation Spectra of Circular, Few-Electron Quantum Dots

L. P. Kouwenhoven, T. H. Oosterkamp, M. W. S. Danoesastro, M. Eto, D. G. Austing, T. Honda, S. Tarucha

SCIENCE • VOL. 278 • 5 DECEMBER 1997

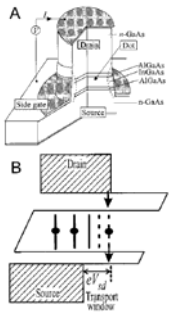

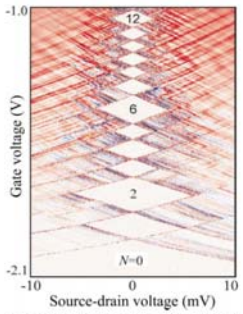

Fig. 2. Differential conductance $\partial I/\partial V_{sd}$ plotted in color scale in the $V_g - V_{sd}$ plane at $B = 0$. In the white diamond-shaped regions, $\partial I/\partial V_{sd} \approx 0$ as a result of Coulomb blockade. N is fixed in each of the diamond regions. The lines outside the diamonds, running parallel to the sides, identify excited states.

Blokada Kulombows

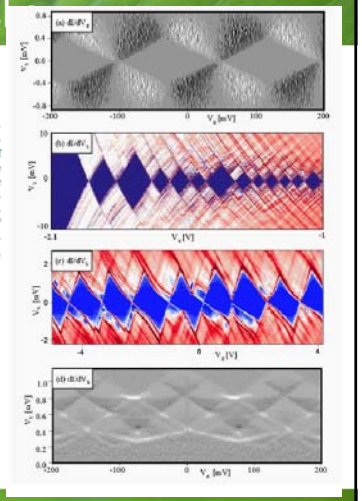

Figure 6.7: The low temperature conductances of (a) a metal single-electron transistor (SET), (b) a semiconducting SET, (c) a carbon nanotube SET, and (d) a superconducting SET are plotted as a function of gate voltage and bias voltage. The diamond shaped regions along the zero bias voltage axis are regions of Coulomb blockade. The conductance is a periodic function of gate voltage for the metal SET and the superconducting SET where the confinement energy is negligible. The conductance is not a periodic function of gate voltage for the semiconductor SET and the carbon nanotube SET where the confinement energy is important. From: P. Hadley and J.E. Mooij, Delft University of Technology, http://qt.tn.tudelft.nl/publi/2000/quantumdev/qdevices.html

Clive Emary
Theory of Nanostructures nanoskript.pdf

Blokada Kulombowska

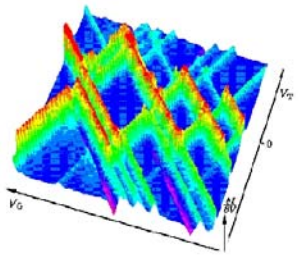

Dodatkowe „diamenty" – np. efekty spinowe , stany wzbudzone itp

http://www-ipcms.u-strasbg.fr/spip.php?article491&lang=en

Figure 1 : The differential conductance, calculated in the regime of sequential tunneling through a one-dimensional quantum dot, as a function of the gate voltage (to the left) and the transport voltage. Green and red: Positive values. Blue: Close to zero. Pink: Negative differential conductance. The Coulomb blockade diamonds are aligned along the gate voltage axis. In parallel, one observes structures which are due to excited states of the dot. Electronic correlations combined with spin selection rules lead to the regions of negative differential conductance.

Blokada Kulombowska

nature physics LETTERS
PUBLISHED ONLINE: 6 APRIL 2009 | DOI: 10.1038/NPHYS1234

Franck–Condon blockade in suspended carbon nanotube quantum dots

Renaud Leturcq[1,2*†], Christoph Stampfer[1,3*], Kevin Inderbitzin[1], Lukas Durrer[1], Christofer Hierold[3], Eros Mariani[4], Maximilian G. Schultz[4], Felix von Oppen[4] and Klaus Ensslin[1]

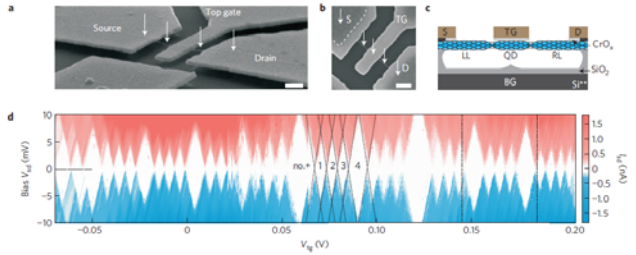

Blokada Kulombowska

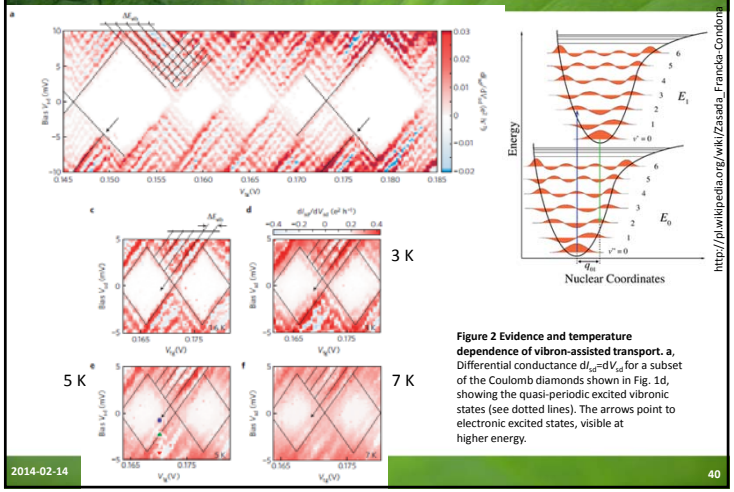

Figure 2 Evidence and temperature dependence of vibron-assisted transport. a, Differential conductance dI_{sd}/dV_{sd} for a subset of the Coulomb diamonds shown in Fig. 1d, showing the quasi-periodic excited vibronic states (see dotted lines). The arrows point to electronic excited states, visible at higher energy.

http://pl.wikipedia.org/wiki/Zasada_Francka-Condona

Blokada Kulombowska

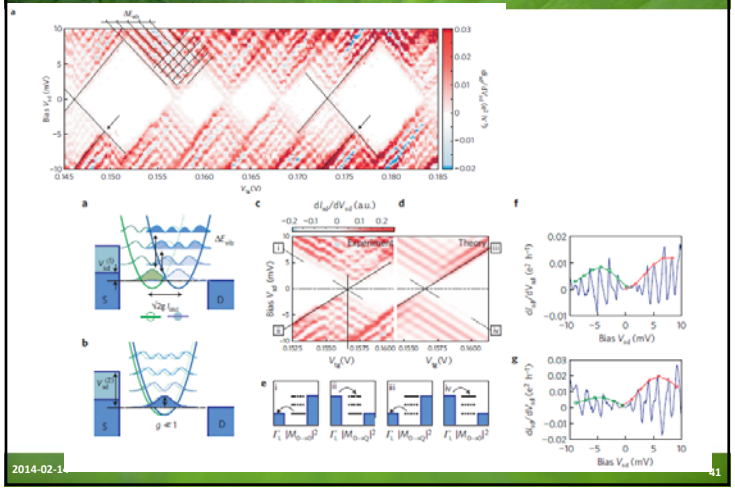

Pojedynczy odczyt pojedynczego spinu

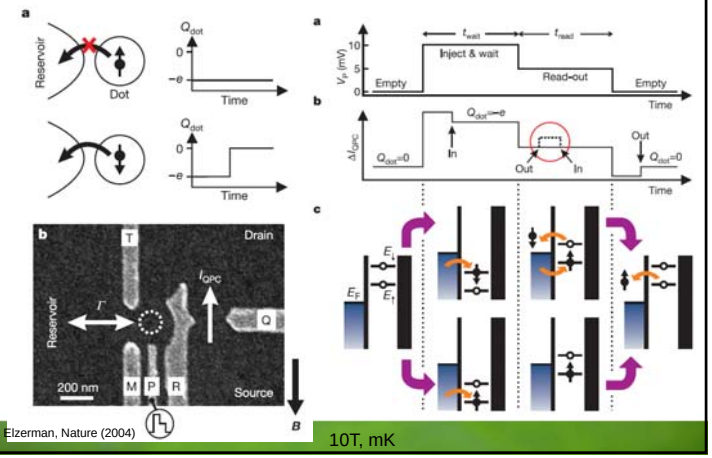

Pojedynczy odczyt pojedynczego spinu

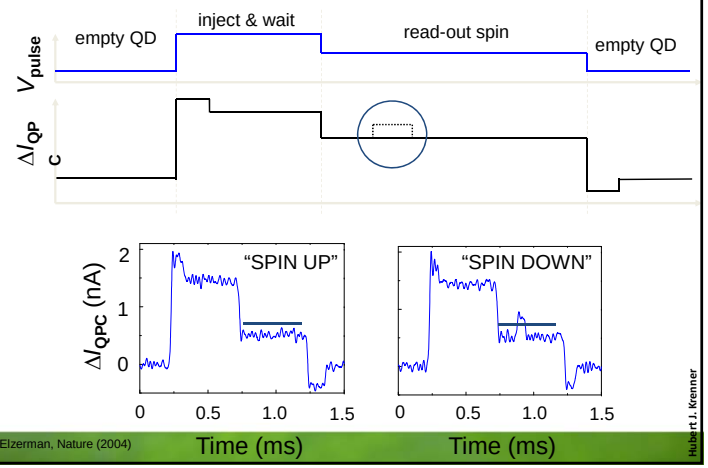

Spin storage

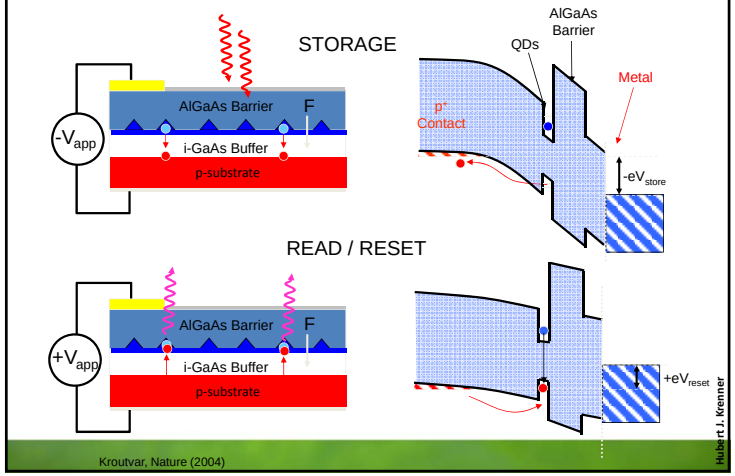

Blokada Kulombowska

ARTICLES nature physics

Anisotropic magneto-Coulomb effects and magnetic single-electron-transistor action in a single nanoparticle

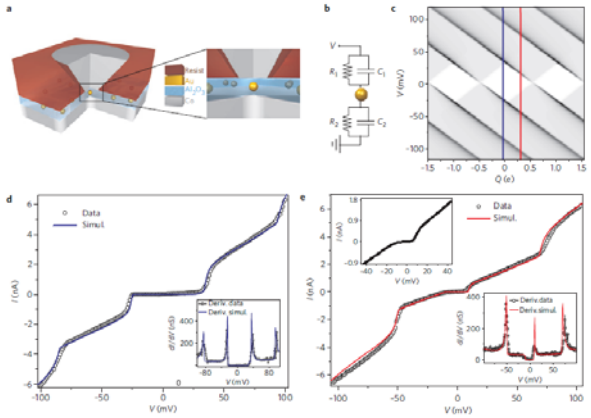

Qubity

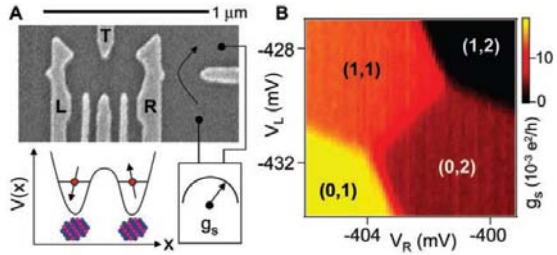

Fig. 1. (A) Scanning electron micrograph of a sample identical to the one measured, consisting of electrostatic gates on the surface of a two-dimensional electron gas. Voltages on gates L and R control the number of electrons in the left and right dots. Gate T is used to adjust the interdot tunnel coupling. The quantum point contact conductance g_s is sensitive primarily to the number of electrons in the right dot. (B) g_s measured as a function of V_L and V_R reflects the double-dot charge stability diagram (a background slope has been subtracted). Charge states are labeled (m,n), where m is the number of electrons in the left dot and n is the number of electrons in the right dot. Each charge state gives a distinct reading of g_s.

Coherent Manipulation of Coupled Electron Spins in Semiconductor Quantum Dots
J. R. Petta, et al. *Science 30 September 2005: 2180-2184.*

Qubity

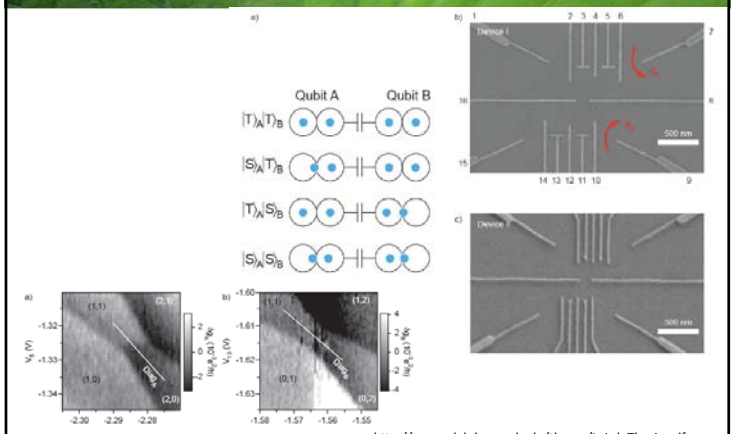

http://marcuslab.harvard.edu/theses/Laird_Thesis.pdf

Qubity

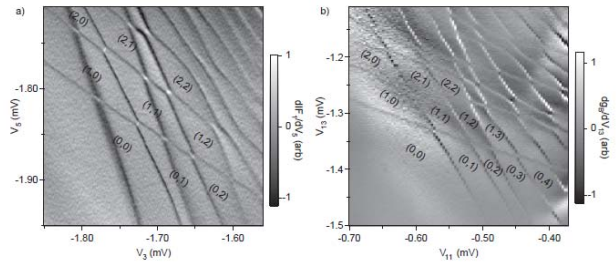

Figure 5.2: Charge stability diagrams of upper (a) and lower (b) double dots, measured using the charge sensors as a function of their respective plunger gate voltages. Both double dots can be tuned into the few-electron regime. The two broad near-vertical lines in (a) are resonances of the charge sensor.

http://marcuslab.harvard.edu/theses/Laird_Thesis.pdf

Tunelowanie

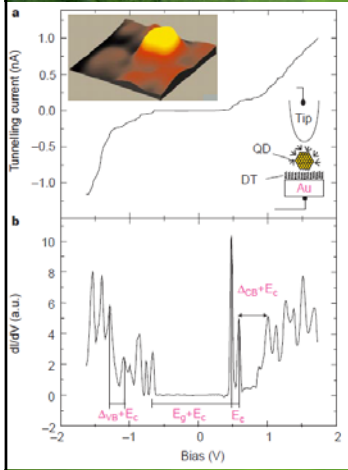

letters to nature

Identification of atomic-like electronic states in indium arsenide nanocrystal quantum dots

Uri Banin*, YunWei Cao*, David Katz† & Oded Millo†

* Department of Physical Chemistry and the Farkas Center for Light Induced Processes, † Raah Institute of Physics, The Hebrew University, Jerusalem 91904, Israel

Figure 1 Scanning tunnelling microscopy and spectroscopy of a single InAs nanocrystal 32 Å in radius, acquired at 4.2 K. The nanocrystal quantum dots (QD) are linked to the gold substrate by hexane dithiol molecules (DT), as shown schematically in the right inset. Left inset, a 10 × 10 nm STM topographic image, showing the nanocrystal. For measuring the *I*–*V* characteristics, the STM tip was positioned above the QD, thus realizing a double-barrier tunnel junction configuration. **a**, The tunnelling *I*–*V* characteristic, exhibiting single-electron tunnelling effects. **b**, The tunnelling conductance spectrum, d*I*/d*V* versus *V*, obtained by numerical differentiation of the *I*–*V* curve (a.u., arbitrary units). The arrows depict the main energy separations: E_c is the single-electron charging energy, E_g is the nanocrystal bandgap, and Δ_{VB} and Δ_{CB} are the spacing between levels in the valence and conduction bands, respectively.

Tunelowanie

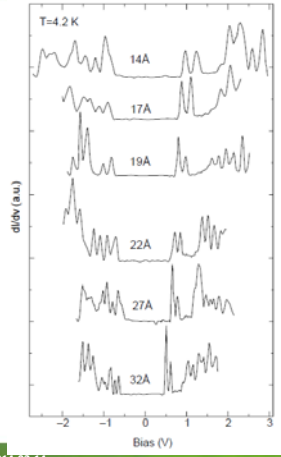

letters to nature

Identification of atomic-like electronic states in indium arsenide nanocrystal quantum dots

Uri Banin*, YunWei Cao*, David Katz† & Oded Millo†

* Department of Physical Chemistry and the Farkas Center for Light Induced Processes, † Raah Institute of Physics, The Hebrew University, Jerusalem 91904, Israel

Figure 2 Size evolution of representative tunnelling d*I*/d*V* versus *V* characteristics, displaced vertically. The position of the centre of the observed zero-current gap showed non-systematic variations with respect to zero bias, of the order of 0.2 eV, probably due to variations of local offset potentials. For clarity of presentation, we offset the spectra along the *V* direction to situate the centres of the observed zero-current gaps at zero bias. The nanocrystal radii are denoted in the figure. The range of displayed voltage for each curve reflects the experimental saturation limit of the detected current.

Tunelowanie

„Kolokwium WAN IN"

1. Znajdź w literaturze parametry pasmowe InAs (masy efektywne, powinowactwo elektr., ε_r) [0p]
2. Na podstawie danych z rys. 1 wyznacz pojemność kropki kwantowej o średnicy 32 A. [5p]
3. Na podstawie rys. 2 oraz 3 wyznacz rozmiar nanocząstek InAs w przybliżeniu **nieskończonej** studni potencjału. Porównaj z wartościami mierzonymi oraz z rys. 3. [10p]
4. Na podstawie rys. 2 oraz 3 wyznacz rozmiar nanocząstek InAs w przybliżeniu **skończonej** studni potencjału. Porównaj z wartościami mierzonymi oraz z rys. 3. [30p] (zadanie numeryczne).
5. Oszacuj powinowactwo elektronowe (electron affinity, energię jonizacji z poziomu studni) oraz pojemność kropek kwantowych z rys. 2. (zadanie numeryczne). Porównaj wyniki z danymi tablicowymi (pkt 1) oraz ze wzorem na pojemność kuli i wyznacz ε_r nanocząstki. [30p]

letters to nature

Identification of atomic-like electronic states in indium arsenide nanocrystal quantum dots

Uri Banin*, YunWei Cao*, David Katz† & Oded Millo†

* Department of Physical Chemistry and the Farkas Center for Light Induced Processes, † Raah Institute of Physics, The Hebrew University, Jerusalem 91904, Israel

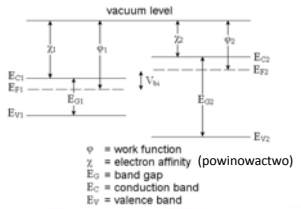

Pola skalarne i wektorowe

Równania Maxwella w ośrodku materialnym

$$\nabla \times \vec{E} = -\frac{\partial \vec{B}}{\partial t}$$

$$\nabla \times \vec{H} = \vec{j}_{sw} + \frac{\partial \vec{D}}{\partial t}$$

$$\nabla \vec{D} = \rho_{sw}$$

$$\nabla \vec{B} = 0$$

Równania materiałowe (linowe)

$$\vec{B} = \mu_0 \vec{H} + \vec{M} = \mu_0(1+\chi_m)\vec{H} = \mu \vec{H} = \mu_r \mu_0 \vec{H}$$

$$\vec{D} = \varepsilon_0 \vec{E} + \vec{P} = \varepsilon_0(1+\chi_e)\vec{E} = \varepsilon \vec{E} = \varepsilon_0 \varepsilon_r \vec{E}$$

$$\vec{j}_{sw} = \hat{\sigma}\vec{E}$$

$$v^2 = \frac{1}{\mu_0 \varepsilon_0}\frac{1}{\mu_r \varepsilon_r} = \frac{c^2}{\mu_r \varepsilon_r} = \frac{c^2}{n^2}$$

Równania zapisane w postaci potencjału skalarnego φ i wektorowego A:

$$\vec{B} = \nabla \times \vec{A}$$

Wtedy $\nabla \times \vec{E} = -\frac{\partial \vec{B}}{\partial t} = -\frac{\partial}{\partial t}(\nabla \times \vec{A}) \Rightarrow \nabla \times \vec{E} + \frac{\partial}{\partial t}(\nabla \times \vec{A}) = 0 \Rightarrow \nabla \times \left(\vec{E} + \frac{\partial \vec{A}}{\partial t}\right) = 0$

Skoro rotacja gradientu znika, to wprowadzamy $-\nabla\varphi = \vec{E} + \frac{\partial \vec{A}}{\partial t}$ czyli $\vec{E} = -\nabla\varphi - \frac{\partial \vec{A}}{\partial t}$

Pola skalarne i wektorowe

Równania Maxwella w ośrodku materialnym

$\vec{B} = \nabla \times \vec{A}$ $\quad$ $\vec{E} = -\nabla\varphi - \frac{\partial \vec{A}}{\partial t}$

Przykładowo: $\varphi = -\vec{E}\vec{r} + C_\varphi \quad \vec{A} = -\vec{E}t + C_A$

Do potencjałów skalarnych i wektorowych możemy dodawać nie tylko stałe C_φ i C_A:

$\varphi \to \varphi - \frac{d\chi}{dt} \quad \vec{A} \to \vec{A} + \nabla\chi$ $\quad$ np.: $\quad \chi = \pm\vec{E}\vec{r}t$

Nazywamy to cechowaniem

Cechowania Landaua: pole $\vec{B} = (0,0,B_z) \Rightarrow B_z = \frac{\partial A_y}{\partial x} - \frac{\partial A_x}{\partial y}$ $\quad A_y = B_z x$ lub $A_x = -B_z y$

(niestety wyróżnia kierunek)

Cechowania Coulomba: $\nabla\vec{A} = 0$ pole $\vec{B} = (0,0,B_z) \Rightarrow \vec{A} = \frac{1}{2}B_z(-y,x,0) = \frac{1}{2}\vec{B} \times \vec{r}$

(niestety komplikuje obliczenia)

Cechowania Lorentza: $\nabla\vec{A} + \frac{\partial\varphi}{\partial t} = 0$

Pola skalarne i wektorowe

Równania Schrodingera w polu $\vec{E}$ i $\vec{B}$:

$\vec{B} = \nabla \times \vec{A}$ $\quad$ $\vec{E} = -\nabla\varphi - \frac{\partial \vec{A}}{\partial t}$

$$\left\{\frac{1}{2m}\left[\hat{p} - q\,\vec{A}(\vec{r},t)\right]^2 + q\varphi(\vec{r},t) + U(\vec{r},t)\right\}\psi(\vec{r},t) = i\hbar\frac{d}{dt}\psi(\vec{r},t)$$

Pęd kanoniczny $\hat{p}$ $\quad$ Suma: pęd kinetyczny

Równanie ciągłości $\quad J(\vec{r},t) = \frac{\hbar\, q}{2\, i\, m}(\Psi^*\nabla\Psi - \Psi\nabla\Psi^*) - \frac{q}{m}|\Psi|^2\vec{A}(\vec{r},t)$

albo:

$$J(\vec{r},t) = \frac{q}{2}\left[\Psi^*\left(\frac{\hat{p} - q\,\vec{A}(\vec{r},t)}{m}\Psi\right) + \left(\frac{\hat{p} - q\,\vec{A}(\vec{r},t)}{m}\Psi\right)^*\Psi\right]$$

Na ćwiczeniach

Pola skalarne i wektorowe

Przykład: stałe pole elektryczne, STUDNIA trójkątna: $\left[-\frac{\hbar^2}{2m}\frac{d^2}{dz^2} + eFz\right]\psi(z) = \varepsilon\psi(z)$

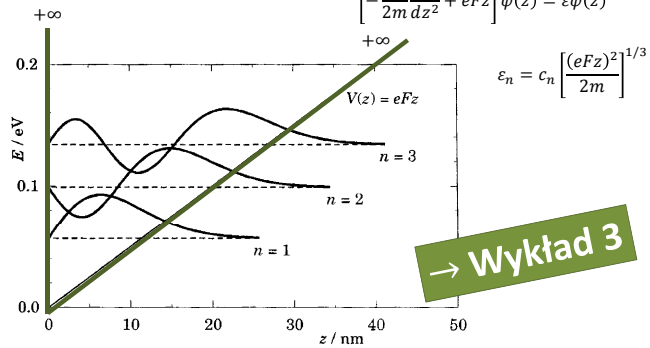

$$\varepsilon_n = c_n\left[\frac{(eFz)^2}{2m}\right]^{1/3}$$

→ Wykład 3

FIGURE 4.6. Triangular potential well $V(z) = eFz$, showing the energy levels and wave functions. The scales are for electrons in GaAs and a field of 5 MV m^{-1}.

Studnia trójkątna

$$\left[-\frac{\hbar^2}{2m}\frac{d^2}{dz^2} + eFz\right]\psi(z) = \varepsilon\psi(z)$$

Przekształcenie:

$$\frac{d^2}{dz^2}\psi(z) = \frac{2m}{\hbar^2}(eFz - \varepsilon)\psi(z)$$

Podstawiamy: $z_0 = \left(\frac{\hbar^2}{2meF}\right)^{1/3}$

$\varepsilon_0 = eFz_0 = \left[\frac{(eF\hbar)^2}{2m}\right]^{1/3}$, $\bar{z} = \frac{z}{z_0}$, $\bar{\varepsilon} = \frac{\varepsilon}{\varepsilon_0}$

$$\frac{d^2}{dz^2}\psi(z) = \frac{2m}{\hbar^2}(eFz - \varepsilon)\psi(z)$$

Równanie typu:

$$\frac{d^2}{dz^2}f(z) = zf(z)$$

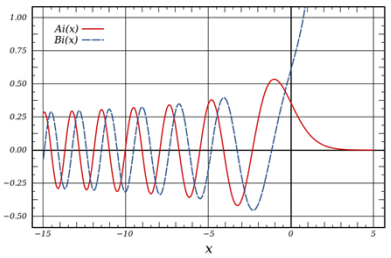

Rozwiązaniem są funkcje Airy $Ai(z)$ i $Bi(z)$. Rozwiązaniami równania są miejsca zerowe funkcji $Ai(z)$ (trzeba tylko najpierw nieco uporządkować równanie).

Pola skalarne i wektorowe

Przykład: stałe pole elektryczne, STUDNIA trójkątna: $\left[-\frac{\hbar^2}{2m}\frac{d^2}{dz^2}+eFz\right]\psi(z)=\varepsilon\psi(z)$

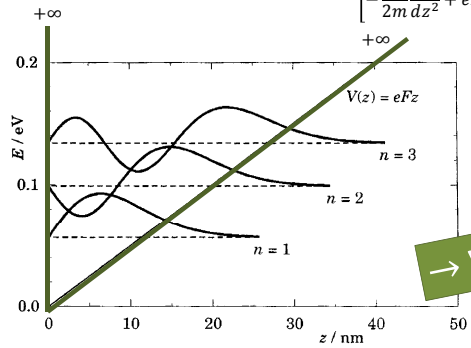

$$\varepsilon_n = c_n\left[\frac{(eFz)^2}{2m}\right]^{1/3}$$

→ Wykład 3

FIGURE 4.6. Triangular potential well $V(z) = eFz$, showing the energy levels and wave functions. The scales are for electrons in GaAs and a field of 5 MV m^{-1}.

Pola skalarne i wektorowe

$\left[-\frac{\hbar^2}{2m}\frac{d^2}{dz^2}+q\varphi(\vec{r},t)\right]\psi(z)=\varepsilon\psi(z)$ Wybieramy cechowanie $q\varphi(\vec{r},t)=eFz$

Rozwiązania STACJONARNE w postaci funkcji Airy:

$$\psi(z,\varepsilon)=Ai\left(\frac{1}{z_0}\left(z-\frac{\varepsilon}{eF}\right)\right)=Ai\left(\frac{eFz-\varepsilon}{\varepsilon_0}\right)$$

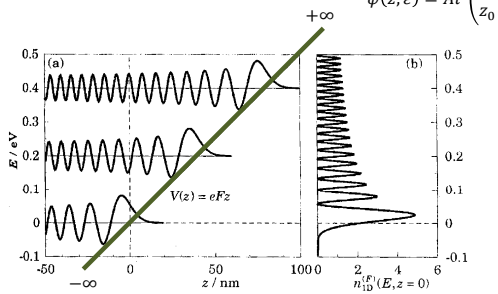

$$\varepsilon_0 = eFz_0 = \left[\frac{(eF\hbar)^2}{2m}\right]^{1/3}$$

$$z_0 = \left(\frac{\hbar^2}{2meF}\right)^{1/3}$$

FIGURE 6.1. (a) Potential energy eFz, three wave functions, and energies for electrons in GaAs in a uniform electric field of 5 MV m^{-1}. (b) Local density of states at $z = 0$, showing how the features correspond to the wave functions.

Pola skalarne i wektorowe

$\left[-\frac{\hbar^2}{2m}\frac{d^2}{dz^2}+q\varphi(\vec{r},t)\right]\psi(z)=\varepsilon\psi(z)$ Wybieramy cechowanie $q\varphi(\vec{r},t)=eFz$

Rozwiązania STACJONARNE w postaci funkcji Airy:

A gdzie jest ruch elektronu w polu???

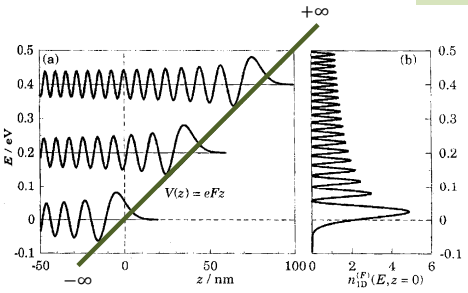

Funkcja falowa

- rozwiązanie przypomina fale stojące!
- funkcja tuneluje w barierę $z > \frac{\varepsilon}{eF}$,
- zanika szybciej dla rosnącego potencjału,
- oscyluje dla $z < \frac{\varepsilon}{eF}$ tym szybciej im $z - \frac{\varepsilon}{eF} \to (-\infty)$, czyli rośnie energia kinetyczna cząsteczki
- Dodanie stałej do potencjału ZMIENIA funkcje falowe!

FIGURE 6.1. (a) Potential energy eFz, three wave functions, and energies for electrons in GaAs in a uniform electric field of 5 MV m^{-1}. (b) Local density of states at $z = 0$, showing how the features correspond to the wave functions.

Lokalna gęstość stanów

Gęstość stanów (ogólnie) można zdefiniować jako:

$$N(E)=\sum_n \delta(E-\varepsilon_n)$$

Jak widać po scałkowaniu:

$$\int_{E_1}^{E_2} N(E)\,dE = \int_{E_1}^{E_2}\sum_n \delta(E-\varepsilon_n)\,dE = \sum_n \int_{E_1}^{E_2}\delta(E-\varepsilon_n)dE$$

Przykładowo:

$$N^{1D}(E)=\sum_k \delta\big(E-\varepsilon(k)\big)=\int \frac{1}{E'(k)}\,\delta(k-k')\,2\,dk=\frac{1}{\pi}\sqrt{\frac{2m}{E}}$$

$$N^{2D}(E)=\sum_k \delta\big(E-\varepsilon(k)\big)=\int \frac{1}{E'(k)}\,\delta(k-k')\,2\pi k\,dk=\frac{m}{\pi\hbar^2}$$

$$N^{3D}(E)=\sum_k \delta\big(E-\varepsilon(k)\big)=\int \frac{1}{E'(k)}\,\delta(k-k')\,4\pi k^2\,dk=\frac{1}{2\pi^2}\left(\frac{2m}{\hbar^2}\right)^{3/2}\sqrt{E}$$

Na ćwiczeniach

Lokalna gęstość stanów

Gęstość stanów (ogólnie) można zdefiniować jako:

$$N(E) = \sum_n \delta(E - \varepsilon_n)$$

Lokalna gęstość stanów:

$$N(E) = \sum_n |\phi_k(\vec{r})|^2 \delta(E - \varepsilon_n)$$

Przykładowo: $N^{1D}(E,z) \sim \int_{-\infty}^{\infty} Ai^2\left(\frac{eFz-\varepsilon}{\varepsilon_0}\right)\delta(E-\varepsilon)\,d\varepsilon \sim \frac{2}{\hbar}\sqrt{\frac{2m}{\varepsilon_0}}Ai^2\left(\frac{eFz-\varepsilon}{\varepsilon_0}\right)$

Lokalna gęstość stanów

Gęstość stanów (ogólnie) można zdefiniować jako:

$$N(E) = \sum_n \delta(E - \varepsilon_n)$$

Lokalna gęstość stanów:

$$N(E) = \sum_n |\phi_k(\vec{r})|^2 \delta(E - \varepsilon_n)$$

Przykładowo: $N^{1D}(E,z) \sim \int_{-\infty}^{\infty} Ai^2\left(\frac{eFz-\varepsilon}{\varepsilon_0}\right)\delta(E-\varepsilon)\,d\varepsilon \sim \frac{2}{\hbar}\sqrt{\frac{2m}{\varepsilon_0}}Ai^2\left(\frac{eFz-\varepsilon}{\varepsilon_0}\right)$

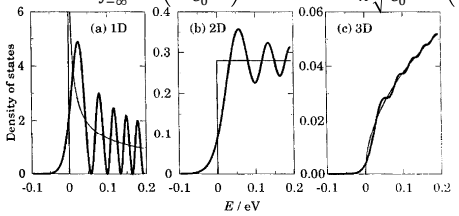

FIGURE 6.2. Local density of states $n^{(F)}(E,z)$ for electrons in GaAs in an electric field of $5\,\mathrm{MV\,m^{-1}}$ as a function of local kinetic energy, $\varepsilon = E - eFz$. The thin curves are the results for free electrons. The units of $n(E,z)$ are $\mathrm{eV^{-1}nm^{-d}}$ in d dimensions.

Lokalna gęstość stanów

Gęstość stanów (ogólnie) można zdefiniować jako:

$$N^{3D}(E,z) \sim \frac{m}{\pi\hbar^3}\sqrt{2m\varepsilon_0}\int_{-\infty}^{E} Ai^2\left(\frac{eFz-\varepsilon}{\varepsilon_0}\right)d\varepsilon = \frac{m}{\pi\hbar^3}\sqrt{2m\varepsilon_0}\left[[Ai'(s)]^2 - s[Ai(s)]^2\right]$$

$$s = \frac{eFz-E}{\varepsilon_0}$$

Przykładowo: $N^{1D}(E,z) \sim \int_{-\infty}^{\infty} Ai^2\left(\frac{eFz-\varepsilon}{\varepsilon_0}\right)\delta(E-\varepsilon)\,d\varepsilon \sim \frac{2}{\hbar}\sqrt{\frac{2m}{\varepsilon_0}}Ai^2\left(\frac{eFz-\varepsilon}{\varepsilon_0}\right)$

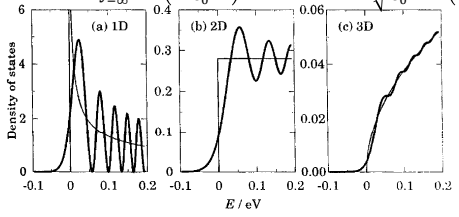

FIGURE 6.2. Local density of states $n^{(F)}(E,z)$ for electrons in GaAs in an electric field of $5\,\mathrm{MV\,m^{-1}}$ as a function of local kinetic energy, $\varepsilon = E - eFz$. The thin curves are the results for free electrons. The units of $n(E,z)$ are $\mathrm{eV^{-1}nm^{-d}}$ in d dimensions.

Lokalna gęstość stanów

Gęstość stanów (ogólnie) można zdefiniować jako:

$$N^{3D}(E,z) \sim \frac{m}{\pi\hbar^3}\sqrt{2m\varepsilon_0}\int_{-\infty}^{E} Ai^2\left(\frac{eFz-\varepsilon}{\varepsilon_0}\right)d\varepsilon = \frac{m}{\pi\hbar^3}\sqrt{2m\varepsilon_0}\left[[Ai'(s)]^2 - s[Ai(s)]^2\right]$$

Efekt Frantza-Kieldysha – w polu elektrycznym przejścia optyczne zachodzą w niższych energiach – bo przerwa energetyczna się „rozmywa" przez tunelowanie do niej stanów:

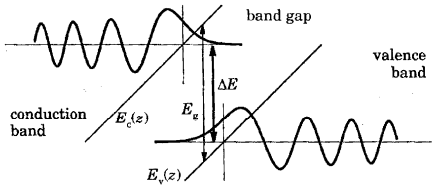

FIGURE 6.3. The Franz–Keldysh effect on interband absorption. The states shown in the valence and conduction bands are separated by $\Delta E < E_g$ but overlap because of the tail that tunnels into the band gap.

Pola skalarne i wektorowe

$$\left[-\frac{\hbar^2}{2m}\frac{d^2}{dz^2}+q\varphi(\vec{r},t)\right]\psi(z)=\varepsilon\psi(z)$$ Wybieramy cechowanie $q\varphi(\vec{r},t)=eFz$

$$\left\{\frac{1}{2m}\left[\hat{p}-q\,\vec{A}(\vec{r},t)\right]^2+q\varphi(\vec{r},t)+U(\vec{r},t)\right\}\psi(\vec{r},t)=i\hbar\frac{d}{dt}\psi(\vec{r},t)$$

Wybieramy cechowanie $\varphi(\vec{r},t)=0$, za to $\vec{A}(\vec{r},t)=-\vec{E}t$

$$\left\{\frac{1}{2m}\left[\hat{p}-e\,\vec{E}t\right]^2\right\}\psi(\vec{r},t)=i\hbar\frac{d}{dt}\psi(\vec{r},t)$$ Nie ma stanów stacjonarnych

Znak −, bo $q=-e$

Potencjał nie zależy od położenia – rozwiązanie typu $\exp(i\,\vec{k}\vec{r})$

$$\psi(\vec{r},t)=\exp(i\,\vec{k}\vec{r})\,\mathrm{T}(\vec{k},t)$$

$$\frac{1}{2m}\left[\hat{p}-e\,\vec{E}t\right]^2\psi_{\vec{k}}(\vec{r},t)=\frac{1}{2m}\left[\hbar\vec{k}-e\,\vec{E}t\right]^2\psi_{\vec{k}}(\vec{r},t)=\frac{\hbar^2}{2m}\left[\vec{k}-\frac{e}{\hbar}\vec{E}t\right]^2\psi_{\vec{k}}(\vec{r},t)=i\hbar\frac{d}{dt}\psi_{\vec{k}}(\vec{r},t)$$

$$\frac{\hbar^2}{2m}\left[\vec{k}-\frac{e}{\hbar}\vec{E}t\right]^2\exp(i\,\vec{k}\vec{r})\,\mathrm{T}(\vec{k},t)=i\hbar\frac{d}{dt}\exp(i\,\vec{k}\vec{r})\,\mathrm{T}(\vec{k},t)$$

Pola skalarne i wektorowe

$$\psi_{\vec{k}}(\vec{r},t)=\exp(i\,\vec{k}\vec{r})\,\mathrm{T}(\vec{k},t)=\exp(i\,\vec{k}\vec{r})\exp\left(-\frac{i}{\hbar}\int^t\frac{\hbar^2}{2m}\left[\vec{k}-\frac{e}{\hbar}\vec{E}t'\right]^2dt'\right)=$$

$$=\exp\left(i\left[\vec{k}\vec{r}-\frac{1}{\hbar}\int^t\frac{\hbar^2}{2m}\left[\vec{k}-\frac{e}{\hbar}\vec{E}t'\right]^2dt'\right]\right)$$

Cząstka przyspiesza w czasie z pędem $\hbar\vec{k}-e\vec{E}t'$, co odpowiada stałej sile $-e\vec{E}$. Pęd cząstki rośnie. Z drugiej strony oczekiwalibyśmy, żeby ta zmiana pędu była widoczna w zmianie przestrzennej $\exp(i\,\vec{k}\vec{r})$ (zmiana długości fali, czyli zmiana wektora falowego $\vec{k}$) - a tego nie ma.

Trudno też zdefiniować gęstość stanów.

Gęstość prądu jest OK – stała w przestrzeni i zwiększa się w czasie (stałe przyspieszenie)

$$J(\vec{r},t)=\frac{q}{2}\left[\Psi^*\left(\frac{\hat{p}-q\,\vec{A}(\vec{r},t)}{m}\Psi\right)+\left(\frac{\hat{p}-q\,\vec{A}(\vec{r},t)}{m}\Psi\right)^*\Psi\right]=-\frac{e}{m}\left(\hbar\vec{k}-e\vec{E}t\right)$$

$$\frac{\hbar^2}{2m}\left[\vec{k}-\frac{e}{\hbar}\vec{E}t\right]^2\exp(i\,\vec{k}\vec{r})\,\mathrm{T}(\vec{k},t)=i\hbar\frac{d}{dt}\exp(i\,\vec{k}\vec{r})\,\mathrm{T}(\vec{k},t)$$

Tensor przewodnictwa

Tensor przewodnictwa: $\vec{j}_{sw}=\hat{\sigma}\vec{E}$ Tensor oporności: $\vec{E}=\hat{\rho}\vec{j}_{sw}$

$$\begin{pmatrix}J_x\\J_y\end{pmatrix}=\begin{pmatrix}\sigma_{xx}&\sigma_{xy}\\\sigma_{yx}&\sigma_{yy}\end{pmatrix}\begin{pmatrix}E_x\\E_y\end{pmatrix}$$

Tensor przewodnictwa: $\vec{j}_{sw}=\hat{\sigma}\vec{E}$

W ośrodku izotropowym $J_x=\sigma_{xx}E_x$

Pola skalarne i wektorowe

Równania Maxwella w ośrodku materialnym

$$\nabla\times\vec{E}=-\frac{\partial\vec{B}}{\partial t}$$

$$\nabla\times\vec{H}=\vec{j}_{sw}+\frac{\partial\vec{D}}{\partial t}$$

$$\nabla\vec{D}=\rho_{sw}$$

$$\nabla\vec{B}=0$$

Równania materiałowe (linowe)

$$\vec{B}=\mu_0\vec{H}+\vec{M}=\mu_0(1+\chi_m)\vec{H}=\mu\vec{H}=\mu_r\mu_0\vec{H}$$

$$\vec{D}=\varepsilon_0\vec{E}+\vec{P}=\varepsilon_0(1+\chi_e)\vec{E}=\varepsilon\vec{E}=\varepsilon_0\varepsilon_r\vec{E}$$

$$\vec{j}_{sw}=\hat{\sigma}\vec{E}$$

$$v^2=\frac{1}{\mu_0\varepsilon_0}\frac{1}{\mu_r\varepsilon_r}=\frac{c^2}{\mu_r\varepsilon_r}=\frac{c^2}{n^2}$$

Równania zapisane w postaci potencjału skalarnego φ i wektorowego A:

$$\vec{B}=\nabla\times\vec{A}$$

Wtedy $\nabla\times\vec{E}=-\frac{\partial\vec{B}}{\partial t}=-\frac{\partial}{\partial t}(\nabla\times\vec{A})\Rightarrow\nabla\times\vec{E}+\frac{\partial}{\partial t}(\nabla\times\vec{A})=0\Rightarrow\nabla\times\left(\vec{E}+\frac{\partial\vec{A}}{\partial t}\right)=0$

Skoro rotacja gradientu znika, to wprowadzamy $-\nabla\varphi=\vec{E}+\frac{\partial\vec{A}}{\partial t}$ czyli $\vec{E}=-\nabla\varphi-\frac{\partial\vec{A}}{\partial t}$

Pola skalarne i wektorowe

Równania Maxwella w ośrodku materialnym

$\vec{B} = \nabla \times \vec{A}$ $\quad$ $\vec{E} = -\nabla\varphi - \frac{\partial \vec{A}}{\partial t}$

Przykładowo: $\varphi = -\vec{E}\vec{r} + C_\varphi \quad \vec{A} = -\vec{E}t + C_A$

Do potencjałów skalarnych i wektorowych możemy dodawać nie tylko stałe C_φ i C_A:

$\varphi \to \varphi - \frac{d\chi}{dt} \quad \vec{A} \to \vec{A} + \nabla\chi$ $\quad$ np.: $\quad \chi = \pm\vec{E}\vec{r}t$

Nazywamy to cechowaniem

Cechowania Landaua: pole $\vec{B} = (0,0,B_z) \Rightarrow B_z = \frac{\partial A_y}{\partial x} - \frac{\partial A_x}{\partial y}$ $\quad A_y = B_z x$ lub $A_x = -B_z y$

(niestety wyróżnia kierunek)

Cechowania Coulomba: $\nabla\vec{A} = 0$ pole $\vec{B} = (0,0,B_z) \Rightarrow \vec{A} = \frac{1}{2}B_z(-y,x,0) = \frac{1}{2}\vec{B} \times \vec{r}$

(niestety komplikuje obliczenia)

Cechowania Lorentza: $\nabla\vec{A} + \frac{\partial\varphi}{\partial t} = 0$

Pola skalarne i wektorowe

Równania Schrodingera w polu $\vec{E}$ i $\vec{B}$:

$\vec{B} = \nabla \times \vec{A}$ $\quad$ $\vec{E} = -\nabla\varphi - \frac{\partial \vec{A}}{\partial t}$

$$\left\{\frac{1}{2m}\left[\hat{p} - q\,\vec{A}(\vec{r},t)\right]^2 + q\varphi(\vec{r},t) + U(\vec{r},t)\right\}\psi(\vec{r},t) = i\hbar\frac{d}{dt}\psi(\vec{r},t)$$

Pęd kanoniczny $\hat{p}$ $\quad$ Suma: pęd kinetyczny

Równanie ciągłości $\quad J(\vec{r},t) = \frac{\hbar\, q}{2\, i\, m}(\Psi^*\nabla\Psi - \Psi\nabla\Psi^*) - \frac{q}{m}|\Psi|^2\vec{A}(\vec{r},t)$

albo:

$$J(\vec{r},t) = \frac{q}{2}\left[\Psi^*\left(\frac{\hat{p} - q\,\vec{A}(\vec{r},t)}{m}\Psi\right) + \left(\frac{\hat{p} - q\,\vec{A}(\vec{r},t)}{m}\Psi\right)^*\Psi\right]$$

Na ćwiczeniach

Pola skalarne i wektorowe

Przykład: stałe pole elektryczne, STUDNIA trójkątna: $\left[-\frac{\hbar^2}{2m}\frac{d^2}{dz^2} + eFz\right]\psi(z) = \varepsilon\psi(z)$

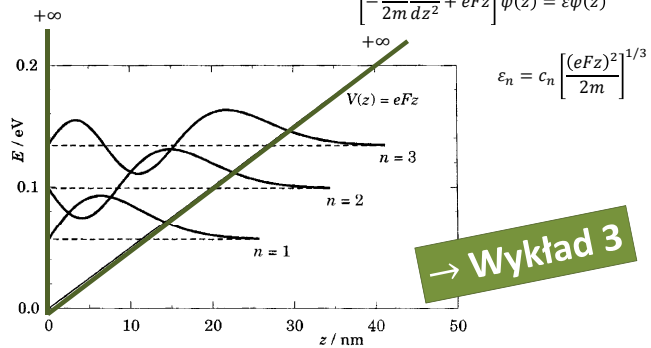

$$\varepsilon_n = c_n\left[\frac{(eFz)^2}{2m}\right]^{1/3}$$

→ **Wykład 3**

FIGURE 4.6. Triangular potential well $V(z) = eFz$, showing the energy levels and wave functions. The scales are for electrons in GaAs and a field of 5 MV m^{-1}.

Studnia trójkątna

$$\left[-\frac{\hbar^2}{2m}\frac{d^2}{dz^2} + eFz\right]\psi(z) = \varepsilon\psi(z)$$

Przekształcenie:

$$\frac{d^2}{dz^2}\psi(z) = \frac{2m}{\hbar^2}(eFz - \varepsilon)\psi(z)$$

Podstawiamy: $z_0 = \left(\frac{\hbar^2}{2meF}\right)^{1/3}$

$\varepsilon_0 = eFz_0 = \left[\frac{(eF\hbar)^2}{2m}\right]^{1/3}$, $\bar{z} = \frac{z}{z_0}$, $\bar{\varepsilon} = \frac{\varepsilon}{\varepsilon_0}$

$$\frac{d^2}{dz^2}\psi(z) = \frac{2m}{\hbar^2}(eFz - \varepsilon)\psi(z)$$

Równanie typu:

$$\frac{d^2}{dz^2}f(z) = zf(z)$$

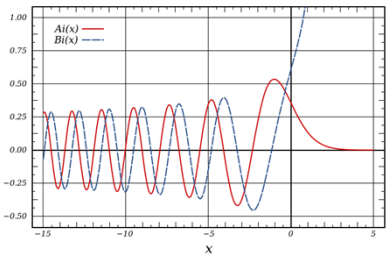

Rozwiązaniem są funkcje Airy $Ai(z)$ i $Bi(z)$. Rozwiązaniami równania są miejsca zerowe funkcji $Ai(z)$ (trzeba tylko najpierw nieco uporządkować równanie).

Pola skalarne i wektorowe

Przykład: stałe pole elektryczne, STUDNIA trójkątna: $\left[-\frac{\hbar^2}{2m}\frac{d^2}{dz^2}+eFz\right]\psi(z)=\varepsilon\psi(z)$

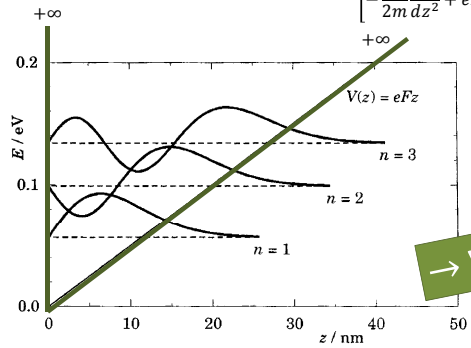

$$\varepsilon_n = c_n\left[\frac{(eFz)^2}{2m}\right]^{1/3}$$

→ Wykład 3

FIGURE 4.6. Triangular potential well $V(z) = eFz$, showing the energy levels and wave functions. The scales are for electrons in GaAs and a field of 5 MV m^{-1}.

Pola skalarne i wektorowe

$\left[-\frac{\hbar^2}{2m}\frac{d^2}{dz^2}+q\varphi(\vec{r},t)\right]\psi(z)=\varepsilon\psi(z)$ Wybieramy cechowanie $q\varphi(\vec{r},t)=eFz$

Rozwiązania STACJONARNE w postaci funkcji Airy:

$$\psi(z,\varepsilon)=Ai\left(\frac{1}{z_0}\left(z-\frac{\varepsilon}{eF}\right)\right)=Ai\left(\frac{eFz-\varepsilon}{\varepsilon_0}\right)$$

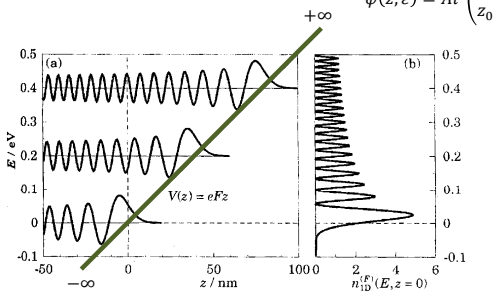

$$\varepsilon_0 = eFz_0 = \left[\frac{(eF\hbar)^2}{2m}\right]^{1/3}$$

$$z_0 = \left(\frac{\hbar^2}{2meF}\right)^{1/3}$$

FIGURE 6.1. (a) Potential energy eFz, three wave functions, and energies for electrons in GaAs in a uniform electric field of 5 MV m^{-1}. (b) Local density of states at $z = 0$, showing how the features correspond to the wave functions.

Pola skalarne i wektorowe

$\left[-\frac{\hbar^2}{2m}\frac{d^2}{dz^2}+q\varphi(\vec{r},t)\right]\psi(z)=\varepsilon\psi(z)$ Wybieramy cechowanie $q\varphi(\vec{r},t)=eFz$

Rozwiązania STACJONARNE w postaci funkcji Airy:

A gdzie jest ruch elektronu w polu???

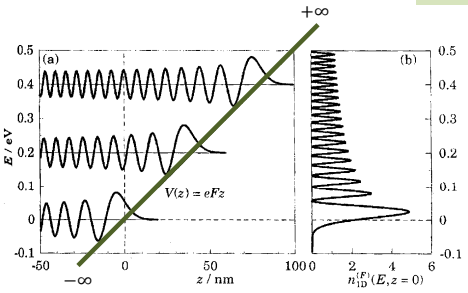

Funkcja falowa

- rozwiązanie przypomina fale stojące!
- funkcja tuneluje w barierę $z > \frac{\varepsilon}{eF}$,
- zanika szybciej dla rosnącego potencjału,
- oscyluje dla $z < \frac{\varepsilon}{eF}$ tym szybciej im $z - \frac{\varepsilon}{eF} \to (-\infty)$, czyli rośnie energia kinetyczna cząsteczki
- Dodanie stałej do potencjału ZMIENIA funkcje falowe!

FIGURE 6.1. (a) Potential energy eFz, three wave functions, and energies for electrons in GaAs in a uniform electric field of 5 MV m^{-1}. (b) Local density of states at $z = 0$, showing how the features correspond to the wave functions.

Lokalna gęstość stanów

Gęstość stanów (ogólnie) można zdefiniować jako:

$$N(E)=\sum_n \delta(E-\varepsilon_n)$$

Jak widać po scałkowaniu:

$$\int_{E_1}^{E_2} N(E)\,dE = \int_{E_1}^{E_2}\sum_n \delta(E-\varepsilon_n)\,dE = \sum_n \int_{E_1}^{E_2}\delta(E-\varepsilon_n)dE$$

Przykładowo:

$$N^{1D}(E)=\sum_k \delta\big(E-\varepsilon(k)\big)=\int \frac{1}{E'(k)}\,\delta(k-k')\,2\,dk=\frac{1}{\pi}\sqrt{\frac{2m}{E}}$$

$$N^{2D}(E)=\sum_k \delta\big(E-\varepsilon(k)\big)=\int \frac{1}{E'(k)}\,\delta(k-k')\,2\pi k\,dk=\frac{m}{\pi\hbar^2}$$

$$N^{3D}(E)=\sum_k \delta\big(E-\varepsilon(k)\big)=\int \frac{1}{E'(k)}\,\delta(k-k')\,4\pi k^2\,dk=\frac{1}{2\pi^2}\left(\frac{2m}{\hbar^2}\right)^{3/2}\sqrt{E}$$

Na ćwiczeniach

Lokalna gęstość stanów

Gęstość stanów (ogólnie) można zdefiniować jako:

$$N(E) = \sum_n \delta(E - \varepsilon_n)$$

Lokalna gęstość stanów:

$$N(E) = \sum_n |\phi_k(\vec{r})|^2 \delta(E - \varepsilon_n)$$

Przykładowo: $N^{1D}(E,z) \sim \int_{-\infty}^{\infty} Ai^2\left(\frac{eFz-\varepsilon}{\varepsilon_0}\right)\delta(E-\varepsilon)\,d\varepsilon \sim \frac{2}{\hbar}\sqrt{\frac{2m}{\varepsilon_0}}Ai^2\left(\frac{eFz-\varepsilon}{\varepsilon_0}\right)$

Lokalna gęstość stanów

Gęstość stanów (ogólnie) można zdefiniować jako:

$$N(E) = \sum_n \delta(E - \varepsilon_n)$$

Lokalna gęstość stanów:

$$N(E) = \sum_n |\phi_k(\vec{r})|^2 \delta(E - \varepsilon_n)$$

Przykładowo: $N^{1D}(E,z) \sim \int_{-\infty}^{\infty} Ai^2\left(\frac{eFz-\varepsilon}{\varepsilon_0}\right)\delta(E-\varepsilon)\,d\varepsilon \sim \frac{2}{\hbar}\sqrt{\frac{2m}{\varepsilon_0}}Ai^2\left(\frac{eFz-\varepsilon}{\varepsilon_0}\right)$

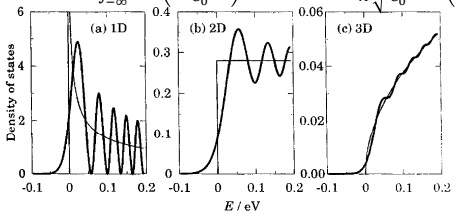

FIGURE 6.2. Local density of states $n^{(F)}(E,z)$ for electrons in GaAs in an electric field of 5 MV m^{-1} as a function of local kinetic energy, $\varepsilon = E - eFz$. The thin curves are the results for free electrons. The units of $n(E,z)$ are eV^{-1}nm^{-d} in d dimensions.

Lokalna gęstość stanów

Gęstość stanów (ogólnie) można zdefiniować jako:

$$N^{3D}(E,z) \sim \frac{m}{\pi\hbar^3}\sqrt{2m\varepsilon_0}\int_{-\infty}^{E} Ai^2\left(\frac{eFz-\varepsilon}{\varepsilon_0}\right)d\varepsilon = \frac{m}{\pi\hbar^3}\sqrt{2m\varepsilon_0}\left[[Ai'(s)]^2 - s[Ai(s)]^2\right]$$

$$s = \frac{eFz-E}{\varepsilon_0}$$

Przykładowo: $N^{1D}(E,z) \sim \int_{-\infty}^{\infty} Ai^2\left(\frac{eFz-\varepsilon}{\varepsilon_0}\right)\delta(E-\varepsilon)\,d\varepsilon \sim \frac{2}{\hbar}\sqrt{\frac{2m}{\varepsilon_0}}Ai^2\left(\frac{eFz-\varepsilon}{\varepsilon_0}\right)$

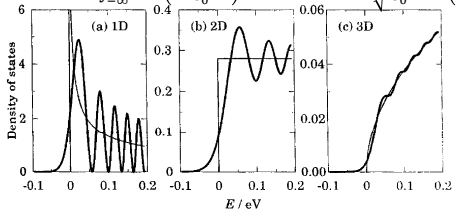

FIGURE 6.2. Local density of states $n^{(F)}(E,z)$ for electrons in GaAs in an electric field of 5 MV m^{-1} as a function of local kinetic energy, $\varepsilon = E - eFz$. The thin curves are the results for free electrons. The units of $n(E,z)$ are eV^{-1}nm^{-d} in d dimensions.

Lokalna gęstość stanów

Gęstość stanów (ogólnie) można zdefiniować jako:

$$N^{3D}(E,z) \sim \frac{m}{\pi\hbar^3}\sqrt{2m\varepsilon_0}\int_{-\infty}^{E} Ai^2\left(\frac{eFz-\varepsilon}{\varepsilon_0}\right)d\varepsilon = \frac{m}{\pi\hbar^3}\sqrt{2m\varepsilon_0}\left[[Ai'(s)]^2 - s[Ai(s)]^2\right]$$

Efekt Frantza-Kieldysha – w polu elektrycznym przejścia optyczne zachodzą w niższych energiach – bo przerwa energetyczna się „rozmywa" przez tunelowanie do niej stanów:

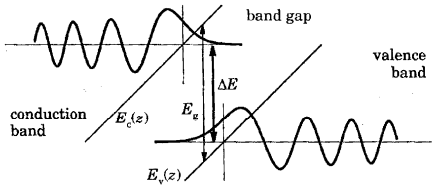

FIGURE 6.3. The Franz–Keldysh effect on interband absorption. The states shown in the valence and conduction bands are separated by $\Delta E < E_g$ but overlap because of the tail that tunnels into the band gap.

Pola skalarne i wektorowe

$\left[-\frac{\hbar^2}{2m}\frac{d^2}{dz^2}+q\varphi(\vec{r},t)\right]\psi(z)=\varepsilon\psi(z)$ Wybieramy cechowanie $q\varphi(\vec{r},t)=eFz$

$\left\{\frac{1}{2m}\left[\hat{p}-q\,\vec{A}(\vec{r},t)\right]^2+q\varphi(\vec{r},t)+U(\vec{r},t)\right\}\psi(\vec{r},t)=i\hbar\frac{d}{dt}\psi(\vec{r},t)$

Wybieramy cechowanie $\varphi(\vec{r},t)=0$, za to $\vec{A}(\vec{r},t)=-\vec{E}t$

$\left\{\frac{1}{2m}\left[\hat{p}-e\,\vec{E}t\right]^2\right\}\psi(\vec{r},t)=i\hbar\frac{d}{dt}\psi(\vec{r},t)$ Nie ma stanów stacjonarnych

Znak −, bo $q=-e$

Potencjał nie zależy od położenia – rozwiązanie typu $\exp(i\,\vec{k}\vec{r})$

$\psi(\vec{r},t)=\exp(i\,\vec{k}\vec{r})\,\mathrm{T}(\vec{k},t)$

$\frac{1}{2m}\left[\hat{p}-e\,\vec{E}t\right]^2\psi_{\vec{k}}(\vec{r},t)=\frac{1}{2m}\left[\hbar\vec{k}-e\,\vec{E}t\right]^2\psi_{\vec{k}}(\vec{r},t)=\frac{\hbar^2}{2m}\left[\vec{k}-\frac{e}{\hbar}\vec{E}t\right]^2\psi_{\vec{k}}(\vec{r},t)=i\hbar\frac{d}{dt}\psi_{\vec{k}}(\vec{r},t)$

$\frac{\hbar^2}{2m}\left[\vec{k}-\frac{e}{\hbar}\vec{E}t\right]^2\exp(i\,\vec{k}\vec{r})\,\mathrm{T}(\vec{k},t)=i\hbar\frac{d}{dt}\exp(i\,\vec{k}\vec{r})\,\mathrm{T}(\vec{k},t)$

Pola skalarne i wektorowe

$\psi_{\vec{k}}(\vec{r},t)=\exp(i\,\vec{k}\vec{r})\,\mathrm{T}(\vec{k},t)=\exp(i\,\vec{k}\vec{r})\exp\left(-\frac{i}{\hbar}\int^t\frac{\hbar^2}{2m}\left[\vec{k}-\frac{e}{\hbar}\vec{E}t'\right]^2dt'\right)=$

$=\exp\left(i\left[\vec{k}\vec{r}-\frac{1}{\hbar}\int^t\frac{\hbar^2}{2m}\left[\vec{k}-\frac{e}{\hbar}\vec{E}t'\right]^2dt'\right]\right)$

Cząstka przyspiesza w czasie z pędem $\hbar\vec{k}-e\vec{E}t'$, co odpowiada stałej sile $-e\vec{E}$. Pęd cząstki rośnie. Z drugiej strony oczekiwalibyśmy, żeby ta zmiana pędu była widoczna w zmianie przestrzennej $\exp(i\,\vec{k}\vec{r})$ (zmiana długości fali, czyli zmiana wektora falowego $\vec{k}$) - a tego nie ma.

Trudno też zdefiniować gęstość stanów.

Gęstość prądu jest OK – stała w przestrzeni i zwiększa się w czasie (stałe przyspieszenie)

$J(\vec{r},t)=\frac{q}{2}\left[\Psi^*\left(\frac{\hat{p}-q\,\vec{A}(\vec{r},t)}{m}\Psi\right)+\left(\frac{\hat{p}-q\,\vec{A}(\vec{r},t)}{m}\Psi\right)^*\Psi\right]=-\frac{e}{m}\left(\hbar\vec{k}-e\vec{E}t\right)$

$\frac{\hbar^2}{2m}\left[\vec{k}-\frac{e}{\hbar}\vec{E}t\right]^2\exp(i\,\vec{k}\vec{r})\,\mathrm{T}(\vec{k},t)=i\hbar\frac{d}{dt}\exp(i\,\vec{k}\vec{r})\,\mathrm{T}(\vec{k},t)$

Tensor przewodnictwa

Tensor przewodnictwa: $\vec{j}_{sw}=\hat{\sigma}\vec{E}$ Tensor oporności: $\vec{E}=\hat{\rho}\vec{j}_{sw}$

$\begin{pmatrix}J_x\\J_y\end{pmatrix}=\begin{pmatrix}\sigma_{xx}&\sigma_{xy}\\\sigma_{yx}&\sigma_{yy}\end{pmatrix}\begin{pmatrix}E_x\\E_y\end{pmatrix}$

Tensor przewodnictwa: $\vec{j}_{sw}=\hat{\sigma}\vec{E}$

W ośrodku izotropowym $J_x=\sigma_{xx}E_x$

Efekt Halla

Siła Lorentza: $\vec{F}=q\vec{v}\times\vec{B}$

Model Drudego: $m^*\left\{\frac{d\vec{v}}{dt}+\frac{\vec{v}}{\tau}\right\}=q\vec{E}+q\vec{v}\times\vec{B}$

τ – czas relaksacji pędowej (*scattering time*)

$m^*\left\{\frac{dv_x}{dt}+\frac{v_x}{\tau}\right\}=qE_x+qv_yB$

$m^*\left\{\frac{dv_y}{dt}+\frac{v_y}{\tau}\right\}=qE_y-qv_xB$

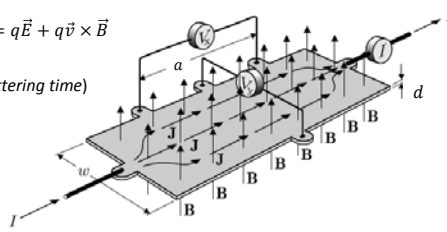

http://www2.physics.ox.ac.uk/sites/default/files/BandMT_11.pdf

Dostajemy:

$v_y\{1+\omega_c^2\tau^2\}=\frac{q\tau}{m^*}\left(E_y-\omega_c\tau E_x\right)$

$\omega_c=\frac{qB}{m^*}$ $\mu=\frac{q\tau}{m^*}$ $j_y=0=\sum_i q_i n v_y^i$

Na ćwiczeniach

Efekt Halla

Zaniedbując $\omega_c^2\tau^2 \ll 1$ i biorąc pod uwagę przewodnictwo elektronów n i dziur p:

$$j_y = 0 = \sum_i q_i n v_y^i$$

$$E_y\{n\mu_c + p\mu_h\} = E_x B\{p\mu_h^2 - n\mu_c^2\}$$

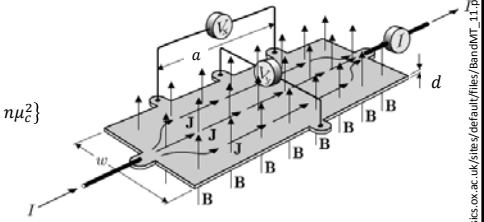

Dostajemy tzw. stałą Halla:

$$R_H = \frac{E_y}{j_x B} = \frac{1}{|e|}\frac{p\mu_h^2 - n\mu_c^2}{(n\mu_c + p\mu_h)^2}$$

Np. dla $p = 0$ mamy $R_H = -\frac{1}{en}$

Na ćwiczeniach

http://www2.physics.ox.ac.uk/sites/default/files/BandMT_11.pdf

Efekt Halla

Biorąc $\sigma_0 = n\,e\,\mu = n\,e^2\,\tau/m$ $\begin{pmatrix} j_x \\ j_y \end{pmatrix} = \begin{pmatrix} \sigma_{xx} & \sigma_{xy} \\ \sigma_{yx} & \sigma_{yy} \end{pmatrix}\begin{pmatrix} E_x \\ E_y \end{pmatrix}$

W przypadku efektu Halla $E = [E_x, 0,0]$:

$j_x = \sigma_{xx}E_x \qquad j_y = \sigma_{yx}E_x$

$$\sigma_{xx} = \frac{\sigma_0}{1+\omega_c^2\tau^2}$$

$$\sigma_{yx} = \frac{\sigma_0\omega_c\tau}{1+\omega_c^2\tau^2}$$

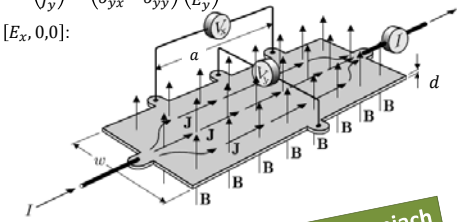

Na ćwiczeniach

Tensor przewodnictwa:

$$\sigma = \begin{pmatrix} \sigma_{xx} & -\sigma_{yx} \\ \sigma_{yx} & \sigma_{xx} \end{pmatrix} = \begin{pmatrix} \sigma_L & -\sigma_T \\ \sigma_T & \sigma_L \end{pmatrix} = \frac{\sigma_0}{1+\omega_c^2\tau^2}\begin{pmatrix} 1 & \omega_c\tau \\ -\omega_c\tau & 1 \end{pmatrix}$$

Tensor oporności: $\rho = \frac{1}{\sigma_L^2 + \sigma_T^2}\begin{pmatrix} \sigma_L & \sigma_T \\ -\sigma_T & \sigma_L \end{pmatrix} = \frac{1}{\sigma_0}\begin{pmatrix} 1 & \omega_c\tau \\ -\omega_c\tau & 1 \end{pmatrix}$

http://www2.physics.ox.ac.uk/sites/default/files/BandMT_11.pdf

Efekt Halla

Pełny tensor przewodnictwa

$$\sigma = ne\mu\begin{pmatrix} \frac{1}{1+s^2} & \frac{-s}{1+s^2} & 0 \\ \frac{s}{1+s^2} & \frac{1}{1+s^2} & 0 \\ 0 & 0 & 1 \end{pmatrix}$$

$s = \frac{eB\tau}{m^*} = \omega_c\tau$

$\mu = \frac{e\tau}{m^*}$

Pełny tensor oporności

$$\rho = \sigma^{-1} = \frac{1}{ne\mu}\begin{pmatrix} 1 & s & 0 \\ -s & 1 & 0 \\ 0 & 0 & 1 \end{pmatrix}$$

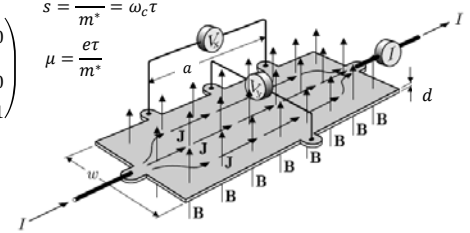

$$\vec{E} = \rho\vec{j} = \begin{bmatrix} \frac{j_x}{ne\mu} \\ -\frac{j_x B}{ne} \\ 0 \end{bmatrix}$$

$$U_{xy} = E_y w = \frac{I_x}{wd}\frac{B}{ne}w = \frac{I_x}{dne}B = R_H\frac{I_x B}{d}$$

$R_H = \frac{1}{ne}$ stała Halla

Efekt Halla

Pełny tensor przewodnictwa

$$\sigma = ne\mu\begin{pmatrix} \frac{1}{1+s^2} & \frac{-s}{1+s^2} & 0 \\ \frac{s}{1+s^2} & \frac{1}{1+s^2} & 0 \\ 0 & 0 & 1 \end{pmatrix}$$

Pełny tensor oporności

$$\rho = \sigma^{-1} = \frac{1}{ne\mu}\begin{pmatrix} 1 & s & 0 \\ -s & 1 & 0 \\ 0 & 0 & 1 \end{pmatrix}$$

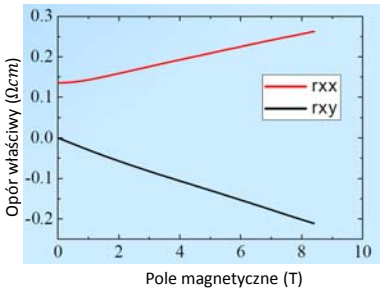

Dla różnych kanałów przewodnictwa

$\sigma = \sum_i \sigma_i$ transport wielonośnikowy – analizujemy tensor σ

Roman Stępniewski

Efekt Halla

Pełny tensor przewodnictwa

$$\sigma = ne\mu \begin{pmatrix} \frac{1}{1+s^2} & \frac{-s}{1+s^2} & 0 \\ \frac{s}{1+s^2} & \frac{1}{1+s^2} & 0 \\ 0 & 0 & 1 \end{pmatrix}$$

Pełny tensor oporności

$$\rho = \sigma^{-1} = \frac{1}{ne\mu} \begin{pmatrix} 1 & s & 0 \\ -s & 1 & 0 \\ 0 & 0 & 1 \end{pmatrix}$$

Dla różnych kanałów przewodnictwa

$$\sigma = \sum_i \sigma_i$$ transport wielonośnikowy

$$R_H = \frac{1}{ne}$$

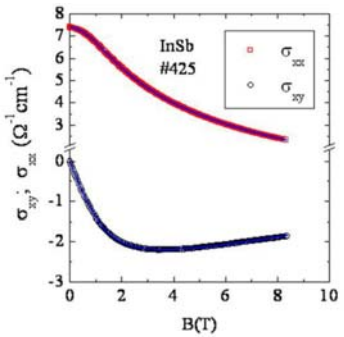

$n_1 = (1.483 \pm .004)10^{16}$ $\mu_1 = (1361. \pm 5)$ cm^2/Vs
$n_2 = (4.60 \pm .02)10^{15}$ $\mu_2 = (4622.6 \pm 9.5)$ cm^2/Vs
$p = (1.77 \pm .06)\ 10^{16}$ $\mu_h = (255 \pm 7)$ cm^2/Vs

Roman Stępniewski

Efekt Halla

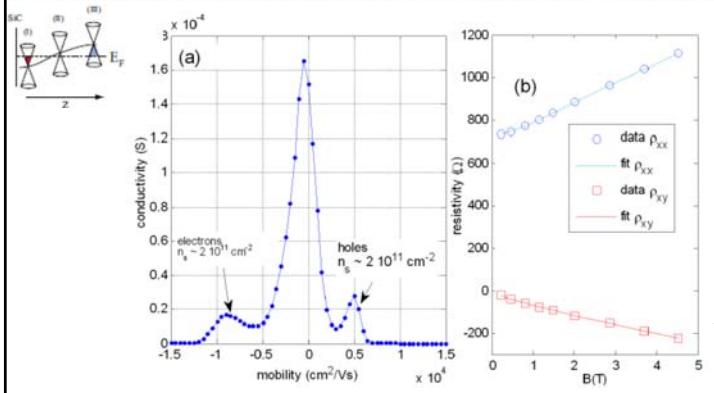

Transport wielonośnikowy w grafenie (M. Gryglas-Borysiewicz)

Roman Stępniewski

Efekt Halla

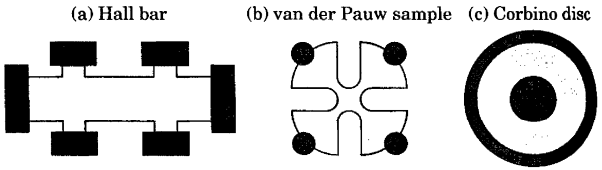

FIGURE 6.5. Samples commonly used for measuring the conductivity of semiconductors: (a) Hall bar, (b) van der Pauw sample, and (c) Corbino disc. The dark areas are the contacts for measuring voltage or current, and the light areas are the active regions of the sample.

$$\sigma = ne\mu \begin{pmatrix} \frac{1}{1+s^2} & \frac{-s}{1+s^2} & 0 \\ \frac{s}{1+s^2} & \frac{1}{1+s^2} & 0 \\ 0 & 0 & 1 \end{pmatrix}$$

$$s = \frac{eB\tau}{m^*} = \omega_c\tau$$

$$\mu = \frac{e\tau}{m^*}$$

Efekt Halla

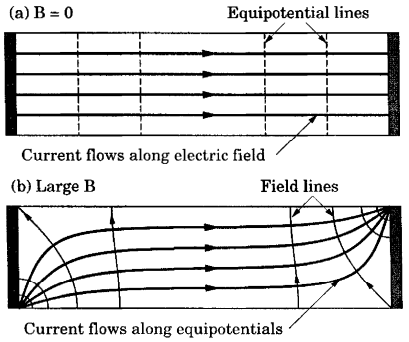

FIGURE 6.6. Electric field, current flow, and equipotentials inside a long rectangular sample with contacts across each end. (a) In the absence of an electric field the current is uniform throughout the sample and runs along the electric field. (b) In a strong magnetic field, where $|\sigma_T| \gg \sigma_L$, the current runs along equipotentials.

Efekt Halla - kwantowy

The Nobel Prize in Physics 1985
Klaus von Klitzing

The Nobel Prize in Physics 1985
Nobel Prize Award Ceremony
Klaus von Klitzing

Klaus von Klitzing

The Nobel Prize in Physics 1985 was awarded to Klaus von Klitzing *"for the discovery of the quantized Hall effect"*.

Efekt Halla - kwantowy

The Nobel Prize in Physics 1998
Robert B. Laughlin, Horst L. Störmer, Daniel C. Tsui

The Nobel Prize in Physics 1998
Nobel Prize Award Ceremony
Robert B. Laughlin
Horst L. Störmer
Daniel C. Tsui

Robert B. Laughlin Horst L. Störmer Daniel C. Tsui

The Nobel Prize in Physics 1998 was awarded jointly to Robert B. Laughlin, Horst L. Störmer and Daniel C. Tsui *"for their discovery of a new form of quantum fluid with fractionally charged excitations"*.

Efekt Halla - kwantowy

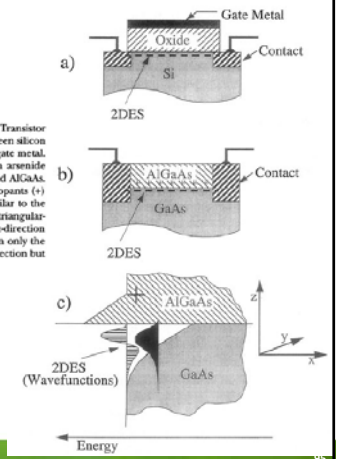

Figure 1 a). Schematic drawings of a silicon Metal Oxide Semiconductor Field Effect Transistor (MOSFET). The two-dimensional electron system (2DES) resides at the interface between silicon and silicon oxide. Electrons are held against the oxide by the electric field from the gate metal. b) Schematic drawings of a modulation-doped gallium arsenide/aluminum gallium arsenide (GaAs/AlGaAs) heterojunction. The 2DES resides at the interface between GaAs and AlGaAs. Electrons are held against the AlGaAs by the electric field from the charged silicon dopants (+) in the AlGaAs. c). Energetic condition in the modulation-doped structure (very similar to the condition in the MOSFET). Energy increases to the left. Electrons are trapped in the triangular-shaped quantum-well at the interface. They assume discrete energy states in the z-direction (black and horizontally striped). At low temperatures and low electron concentration only the lowest (black) electron state is occupied. The electrons are totally confined in the z-direction but can move freely in the x-y-plane.

Horst Stormer, *Nobel Lecture*

Efekt Halla - kwantowy

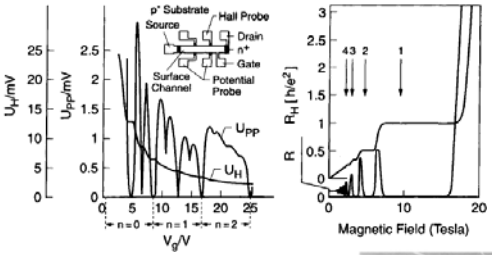

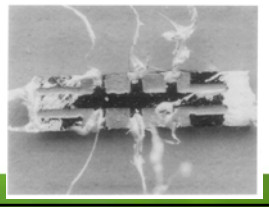

Horst Stormer, *Nobel Lecture*

Efekt Halla - kwantowy

VOLUME 45, NUMBER 6 PHYSICAL REVIEW LETTERS 11 AUGUST 1980

New Method for High-Accuracy Determination of the Fine-Structure Constant Based on Quantized Hall Resistance

K. v. Klitzing
Physikalisches Institut der Universität Würzburg, D-8700 Würzburg, Federal Republic of Germany, and Hochfeld-Magnetlabor des Max-Planck-Instituts für Festkörperforschung, F-38042 Grenoble, France

and

G. Dorda
Forschungslaboratorien der Siemens AG, D-8000 München, Federal Republic of Germany

and
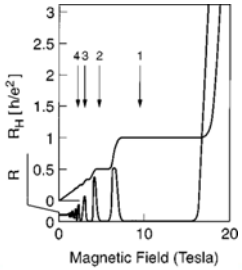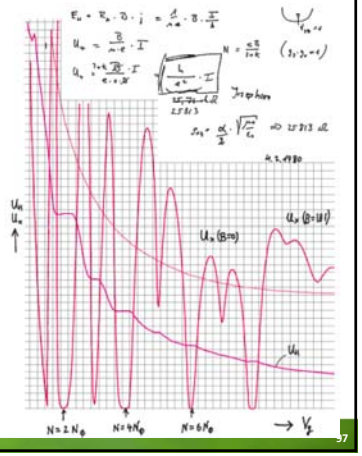
M. Pepper
Cavendish Laboratory, Cambridge CB3 0HE, United Kingdom
(Received 20 May 1980)